Journal of Medicinal Chemistry

Article

Discovery of a Novel Dual Histone Deacetylases (HDACs) and Mammalian Target of Rapamycin (mTOR) Target Inhibitor as a Promising Strategy for Cancer Therapy

Yong Chen, Xue Yuan, Wanhua Zhang, Minghai Tang, Li Zheng, Fang Wang, Wei Yan, Shengyong Yang, Yuquan Wei, Jun He, and LiJuan Chen

J. Med. Chem., **Just Accepted Manuscript** • DOI: 10.1021/acs.jmedchem.8b01825 • Publication Date (Web): 10 Jan 2019

Discovery of a Novel Dual Histone Deacetylases (HDACs) and Mammalian Target of Rapamycin (mTOR) Target Inhibitor as a Promising Strategy for Cancer Therapy

Yong Chen[a,§], Xue Yuan[a,§], Wanhua Zhang[b,§], Minghai Tang[a], Li Zheng[a], Fang Wang[a], Wei Yan[a], Shengyong Yang[a], Yuquan Wei[a], Jun He [a,*], Lijuan Chen[a,*]

[a] State Key Laboratory of Biotherapy/Collaborative Innovation Center of Biotherapy and Cancer Center, West China Hospital of Sichuan University, Chengdu, 610041, China.

[b] Department of Hematology and Research Laboratory of Hematology, West China Hospital of Sichuan University, Chengdu, 610041, China.

[§] These authors contributed equally and should be considered as co-first author

Abstract

In the present study, a series of novel dual target HDAC and mTOR inhibitors were designed and synthesized, using pyrimidine-pyrazolyl pharmacophore to append HDAC recognition cap and hydroxamic acid as a zinc-binding motif. Among them, **12l** was the optimal lead compound with potent inhibition activities against mTOR and HDAC1 with IC_{50} of 1.2 nM and 0.19 nM. Western blot confirmed that **12l** could upregulate acetylation of H3 and α-tubulin and downregulate mTOR related downstream mediators. **12l** could also stimulate cell cycle arrest in G_0/G_1 phase and induce tumor cell apoptosis. **12l** showed comparable anti-tumor activity with the combination medication in MM1S xenograft model with TGI of 72.5%, without causing significant loss of body weight and toxicity. All the results indicated that **12l** could be a promising dual target inhibitor for treating hematologic malignancies.

Introduction

The mammalian target of rapamycin (mTOR) regulates cell growth and survival by integrating both extracellular and intracellular signals[1, 2]. These signaling functions are distributed in distinct multiprotein complexes: mTOR complex 1 (mTORC1) and mTOR complex 2 (mTORC2)[3]. mTOR is a downstream mediator of the PI3K/Akt pathway that is over activated in numerous tumors. mTORC1 is sensitive to rapamycin, while mTORC2 is resistant to rapamycin because of rapamycin triggering a negative feedback mechanism by activating survival pathways involving Akt and eIF4e, which may limit the anti-cancer efficacy[1, 4-6]. Several dual mTORC1 and mTORC2 inhibitors, such as AZD8055[7, 8], Torkinib (PP242)[4], CC223[9], not only

inhibit multisite eIF4E-bing protein 1 (4E-BP1) phosphorylation but also block PI3K/Akt negative feedback[10]. They belong to second-generation ATP competive inhibitors and more effective than first-generation inhibitors. However, mTOR resistance mutations, mainly including FRB mutations and kinase domain mutations, led to poor therapeutical effects and prognosis in clinical applications[11]. Numerous reports revealed that histone deacetylases (HDACs) are considered to be among the most promising targets for cancer therapy, and four HDAC inhibitors have been approved by FDA for treating hematologic malignancies[12-17]. Researchers tried to adopt a combination treatment strategy of mTOR and HDAC inhibitors for treating relapsed/refractory lymphoma in recent years[18, 19]. Emerging data indicated that mTOR inhibitors were more effective when combined with HDAC inhibitors due to synergy effects[18, 20-24]. One report demonstrated that panobinostat (LBH-589) and everolimus (RAD001) combination resulted in enhanced anti-tumor efficacy mediated by decreasing tumor growth concurrent with augmentation of p21 and p27 expression and the attenuation of angiogenesis and tumor proliferation via androgen receptor, c-Myc and HIF-1α signaling[16, 22]. Moreover, panobinostat could overcome rapamycin-mediated resistance by inhibiting Akt signaling through mTORC2[25]. Such promising research drew our attention to develop novel and highly effective small molecule inhibitors of dual mTOR and HDAC targets. Up to now, no dual mTOR and HDAC target inhibitors are available in clinical or on market. Our research groups decided to design a series of novel target molecules in order to develop a dual mTOR and HDAC inhibitor. Many researchers utilized pyrimidine-pyrazolyl analogues as

stem nucleus to develop several effective mTORC1/mTORC2 inhibitors, such as PP242, AZD8055 and Sapanisertib (INK128)[26]. Hydroxamic acid is the most common zinc binding group (ZBG) moiety in HDAC inhibitors owing to its ability to reliably chelate active-site zinc ions by far[24, 25], such as LBH-589, Vorinostat (SAHA), Ricolinostat (ACY1215)[27]. We thought of designing pyrimidine-pyrazolyl pharmacophore to append HDAC recognition cap and hydroxamic acid as a zinc binding motif (Figure 1). A series of compounds were synthesized and evaluated for the cell inhibition activities and (or) enzymatic inhibition activities. As expected, **12l** potently inhibited mTOR and HDAC1 with IC_{50} values of 1.2 nM and 0.19 nM, respectively. Western blot analysis reconfirmed dual inhibition on HDACs and mTOR kinase in a concentration dependent manner. **12l** could stimulate cell cycle arrest in G_0/G_1 phase and induce tumor cell apoptosis. And in vivo anti-tumor activity in xenograft models suggested that **12l** could be a suitable drug candidate for treating hematologic malignancies.

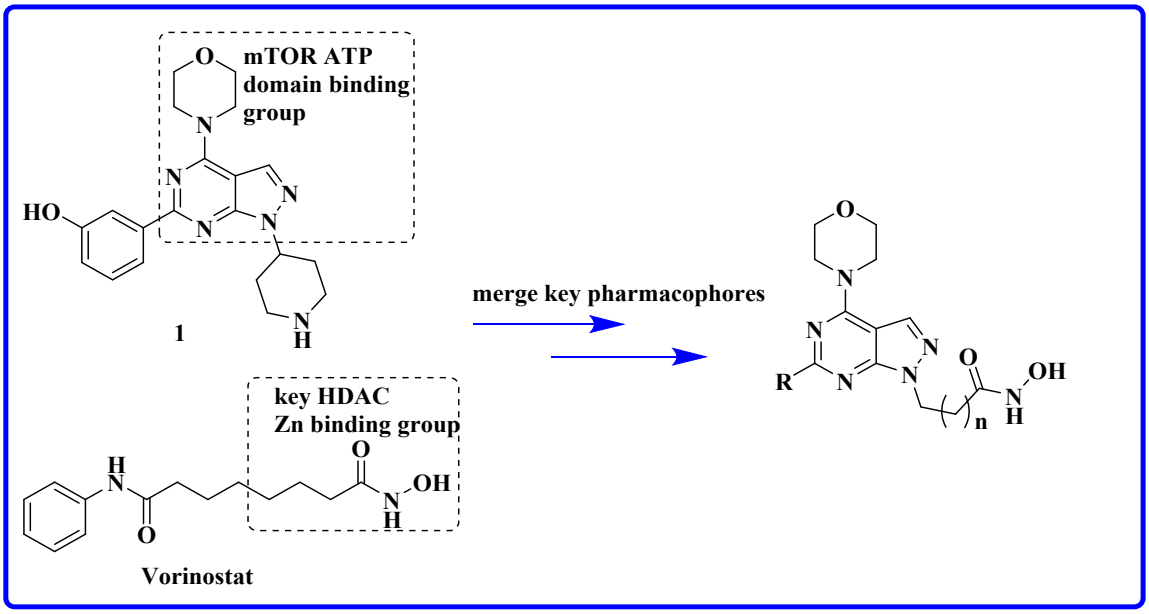

Figure 1. Schematic showing plans for merged mTOR-HDAC pharmacophore taking

advantage of ATP domain binding group and HDAC zinc binding group[1].

Results and Discussion

Chemistry

The general procedure to synthesize the target molecules **6a-i** has been outlined in Scheme 1. Commercially available 4,6-dichloro-1*H*-pyrazolo[3,4-*d*]pyrimidine (**1**) as the starting material reacted with morphline to give **2**. Under N_2 atmosphere protection, **2** was treated with morphline/*N*-methylpiperazine to obtain **3**/**4** The compound **3**/**4** was introduced an aliphatic chain group by reacting with bromoacetate analogues, which got the corresponding compounds **5a-g** and **5h-i** (**3** was treated with methyl 3-(4-bromomethyl)cinnamate to get **5j**). These compounds were directly converted into targets molecules **6a-j** by NH_2OH.

Scheme 1. Syntheses of compounds **6a-i**.[a]

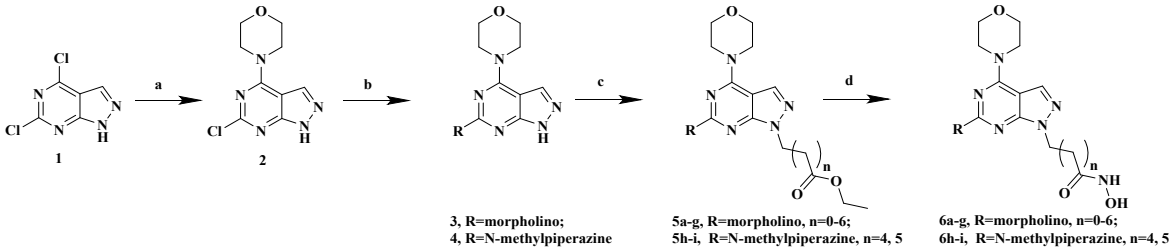

[a] Reagents and Conditions: (a) morphline, CH_3OH, rt, 0.5 h; (b) morphline/*N*-methylpiperazine, DIEA, KI, NMP, 90 °C, 8 h; (c) $BrCH_2(CH_2)_nCOOEt$, n = 0-6, Cs_2CO_3, DMF, 120 °C, MW, 1 h; (d) NH_2OH, NaOH, CH_3OH/CH_2Cl_2, 1 h.

In Vitro Cell Growth Inhibitory Effects of Compounds 6a-j. We primarily began our research by screening the inhibitory activities of these compounds in HCT116 and Ramos cells. We first tested two concentrations in both cells including 5 μM and 0.5 μM, and the data was shown in Table 1. The inhibition rate below 50 % can be

considered to be ineffective or inefficient. Obviously, compounds **6a-c** showed no inhibitory activities at two concentrations in HCT116 and Ramos cells. When the chain length of the linker region became three carbon atoms, compound **6d** exhibited weak inhibitory activity at 5 μM. Similarly, compound **6e** slightly improved inhibitory activity and the inhibition rate was > 60 % at 0.5 μM. Not surprisingly, compound **6f** showed higher efficiency in two cells even at 0.5 μM. However, compound **6g** which contained seven carbon atoms in linker region sharply reduced inhibitory activities at 0.5 μM. Meantime, compounds **6h** and **6i** also showed equivalent inhibitory activities in HCT116 cells, especially remarkable inhibitory efficacy in Ramos cells. Compound **6j** consisting of vinylbenzene instead of aliphatic chain also showed weak activity inferior to **6f**. These results suggested that six carbon atoms chain of the linker region was the optimal group to maintain the inhibitory activities in solid and hematological cancer cells.

Table 1. Cell growth inhibition rate of compounds **6a-j** in HCT116 and Ramos cells.

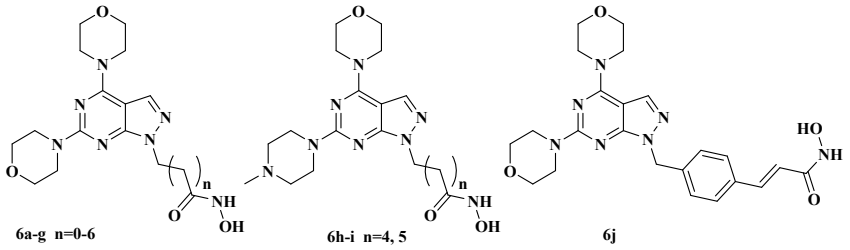

Compd	n	inhibition rate (%) [a]			
		HCT116		Ramos	
		5 μM	0.5 μM	5 μM	0.5 μM
6a	0	18.1	3.5	12.4	1.1
6b	1	22.4	6.3	15.7	8.5
6c	2	30.1	15.7	39.6	20.5
6d	3	55.8	22.6	60.2	33.3

6e	4	92.1	62.4	94.6	69.2
6f	5	95.2	92.9	97.4	91.0
6g	6	71.8	13.8	99.1	26.9
6h	4	56.9	10.2	99.5	91.2
6i	5	80.3	59.9	99.5	90.1
6j		59.5	12.0	98.2	16.8

[a] The inhibition rate values are the means of at least two experiments.

To search the structure and activity relationship (SAR) of cap with the fixed linker region, we also synthesized compounds **10a-j** (Scheme 2). The synthetic route was similar to Scheme 1, compound **2** reacted with ethyl 7-bromoheptanoate to give **7**. Then **7** was introduced kinds of aromatic nucleus by Suzuki coupling reaction to obtain **9a-j**. These compounds were also directly converted into target molecules **10a-j** by NH_2OH.

Scheme 2. Syntheses of compounds **10a-j**.[a]

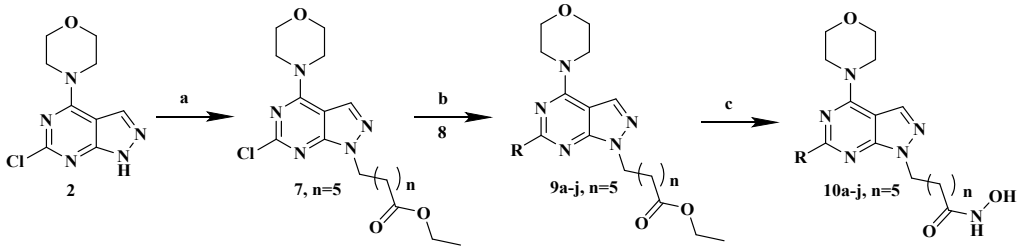

[a] Reagents and Conditions： (a) $Br(CH_2)_6COOEt$, Cs_2CO_3, DMF, MW, 1 h; (b) boronic acid derivatives, Dioxane/EtOH/water(v/v/v, 7/3/4), 80 °C, 2 h; (c) NH_2OH, NaOH, CH_3OH/CH_2Cl_2, 1 h.

In Vitro Cell Growth Inhibitory Effects of Compounds 10a-j. On the basis of the former researches and discussions, compounds with C-2 position modification were chosen to further evaluate cell growth inhibitory effects in different cancer cells,

including HCT116, Raji, MCF-7 and MM1S cells. In view of the inhibition rates of **6f** in HCT116 and Ramos cells, we directly tested the IC_{50} values in the four cancer cells. Though compound **6f** showed high efficacy at 0.5 μM, the highest inhibition activity (IC_{50}) in HCT116 was only 89.9 nM and IC_{50} values were >100 nM in other cancer cells. Satisfactorily acceptably, compound **10a** with anilino group at C-2 position exhibited remarkable inhibition activities in four cancer cells. Dramatically, the IC_{50} values toward HCT116 and Raji were 7.0 nM and 7.1 nM, respectively. However, **10c** exhibited equivalent effects in hematological tumors but worse activities toward solid tumor cells when pyridyl replaced phenyl. When phenyl was replaced by pyrimidinyl (**10b**), the inhibition activities sharply declined in tested tumor cells. And **10f** almost lost inhibition activities in comparison with **10a**. We can draw conclusion that phenyl group contributed to increasing inhibition activities toward these cancer cells. Predictably, **10e** showed better inhibitory activities than **10d** but inferior to **10a**. In addition, amino group played an important role in maintaining potent inhibition activities statistically. When five-membered heterocycle groups were introduced at C-2 position (**10h**, **10i** and **10j**), the inhibition activities in hematological tumors still remained at nM level but inferior to **10a**. **10a** with aniline group at C-2 position was preferred pilot structure with excellent cell inhibitory effects in solid and hematological tumor cells. Moreover, the research outcome was in accordance with our previous conclusion.[28]

Table 2. IC_{50} values in several cancer cells of compounds **10a-j**, **6f** and SAHA.

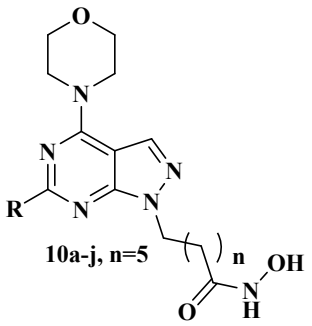

Compd	R	IC_{50} ± SEM [a], nM			
		HCT116	Raji	MCF-7	MM1S
6f		89.9 ± 14.5	158.6 ± 30.6	371.9 ± 14.3	192.3 ± 32.9
10a	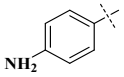	7.1 ± 1.8	7.1 ± 2.6	63.7 ± 6.7	18.9 ± 1.5
10b	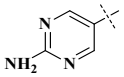	163 ± 10	31.7 ± 2.3	221 ± 5.4	32.6 ± 1.6
10c	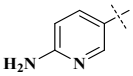	61.3 ± 8.1	7.1 ± 0.2	163 ± 6	8.4 ± 1.9
10d	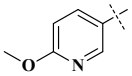	66.9 ± 7.8	44.9 ± 10.4	372.4 ± 52.6	> 500
10e	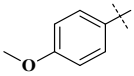	38.0 ± 2.0	29.3 ± 9.7	70.6 ± 17.5	353.5 ± 83.5
10f		296.3 ± 62.8	> 500	> 500	> 500
10g	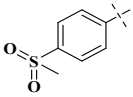	76.5 ± 7.0	111.4 ± 5.4	> 500	168.1 ± 4.3
10h		34.9 ± 0.6	7.7 ± 0.2	156 ± 3.6	15.6 ± 1.3
10i		106.9 ± 40.6	15.3 ± 2.1	180.4 ± 57.3	52.3 ± 3.0
10j		72.8 ± 2.7	14.6 ± 0.4	202 ± 5	35.6 ± 0.4
SAHA		882.5 ± 66.5	196 ± 7	354 ± 2	573 ± 9

[a] IC_{50} = compound concentration required to inhibit tumor cell proliferation by 50%; data are expressed as the mean ± SEM from the dose-response curves of at least three independent experiments.

In Vitro Enzymatic Inhibitory Effects for PI3Kα and mTOR. Owing to most HDAC inhibitors acting on hematological cancers and in view of several compounds showing remarkable inhibitory activities in hematological cancer cells, we decided to test enzymatic inhibitory effects for mTOR first. Moreover, PI3K kinases are the upstream signal mediators of mTOR. PI3Kα and mTOR kinases targets were chosen to test these compounds and data was shown in Table 3. Obviously, all these compounds hardly inhibited PI3Kα kinase. However, several compounds could partially inhibit mTOR, such as **10a** whose inhibition rate was 95% and **10i** with 85% inhibition rate at 500 nM. Theoretically, **10a** may be an efficient mTOR inhibitor which needed subsequent specific data.

Table 3. Enzymatic inhibition rate for PI3Kα and mTOR.

Compd	inhibition rate (%) at 500 nM [a]	
	PI3Kα	mTOR
6a	5.9 ± 2.7	-12 ± 2.1
6b	11 ± 1.7	-5.0 ± 0.5
6c	17 ± 1.6	21 ± 0.5
6d	15 ± 3.7	-5.4 ± 4.5
6e	1.0 ± 0.1	-4.2 ± 0.4
6f	4.5 ± 2.1	2.2 ± 2.3
6g	-1.2 ± 0.7	4.4 ± 0.7
6h	1.5 ± 0.8	-1.7 ± 1.6
6i	-6.2 ± 0.8	-0.4 ± 1.4
6j	-3.0 ± 1.3	-5.4 ± 1.7
10a	16 ± 1.6	95 ± 0.2
10b	1.2 ± 0.7	40 ± 1.1
10c	1.9 ± 0.8	35 ± 0.9

10d	3.3 ± 5.7	58 ± 1.0
10e	-1.0 ± 1.5	38 ± 2.3
10f	-0.1 ± 0.3	17 ± 7.4
10g	31 ± 4.6	64 ± 1.5
10h	8.4 ± 1.1	35 ± 2.9
10i	-3.8 ± 1.0	85 ± 0.0
10j	9.7 ± 5.6	55 ± 3.2

[a] The inhibition rate values are the means of at least two experiments.

Then IC_{50} values of **10a** for HDACs and mTOR were evaluated. The results were shown in Table 4. As expected, **10a** showed excellent inhibition activities toward HDACs. The IC_{50} values were 0.21 nM, 1.6 nM, 4.21 nM for HDAC 1, 2, 3 and 2.43 nM, 1.43 nM for HDAC 6, 10, respectively. Moreover, the IC_{50} values for HDAC 4, 5, 7, 9, and 11 were > 1 μM. The result indicated **10a** was a class I and class IIb selective HDAC inhibitor. **10a** also exhibited potent inhibition effect for mTOR kinase with IC_{50} of 40 nM. By far, **10a** was selected out to be an acceptable dual HDAC and mTOR inhibitor. Improvement of inhibition efficacy for mTOR kinase need further structure modification and optimization based on lead compound **10a**.

Table 4. IC_{50} values for HDACs and mTOR of compound **10a**.

	Class I				**Class IIb**		
	HDAC1	**HDAC2**	**HDAC3**	**HDAC8**	**HDAC6**	**HDAC10**	**mTOR**
IC_{50},nM	0.21	1.60	4.21	35.67	2.43	1.43	40

[a] IC_{50} values for enzymatic inhibition of HDACs and mTOR kinase. The IC_{50} values are the means of at least two experiments, with intra- and inter- assay variations of <

10%.

As reported, introduction of urea linkage to aniline could improve inhibition efficacy for mTOR kinase[1]. We adopted the similar strategy and **12a-p** were designed and synthesized. **9a** was acylated by triphosgene and then RNH or RNH_2 was added to give urea intermediates **11a-p**. These compounds were also directly converted into target molecules **12a-p** by NH_2OH.

Scheme 3. Syntheses of compounds **12a-p**.[a]

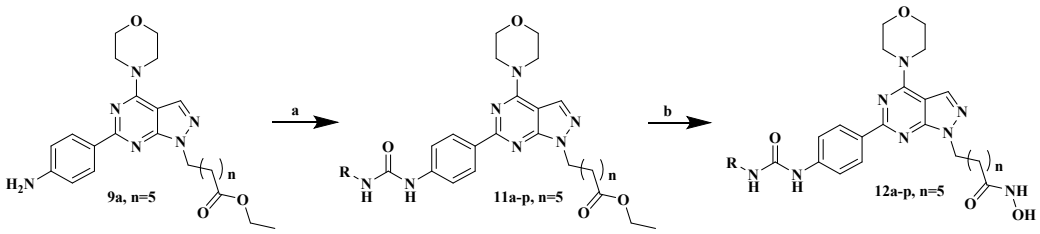

[a] Reagents and Conditions: (a) triphosgene, NEt_3, CH_2Cl_2; RNH or RNH_2; (b) NH_2OH, NaOH, CH_3OH/CH_2Cl_2, 1 h.

To validate our design strategy of improving cell inhibition activities, compounds **12a-p** were first evaluated IC_{50} values in HCT116, Raji, and MM1S cell lines. The data was outlined in Table 5. **12a** promoted inhibition efficacy in hematological tumor cells with IC_{50} values of 3.5 nM, 13.4 nM for Raji and MM1S, respectively. When ethyl was introduced (**12b**), the inhibition effect was inferior to **12a** and **10a**. However, the inhibition activity of **12c** for tested cells with propyl substituent decreased sharply. The potency performed differently when various short aliphatic chains were introduced but all inferior to **12a**. Additionally, aromatic rings (**12g**, **12h**, **12i**, and **12j**) were inserted instead of aliphatic chains. **12g** and **12h** exhibited equivalent inhibition activities both in solid and hematological tumor cells with

average IC_{50} value of 20 nM. Trialkylamine as one domain of urea was introduced to obtain compounds **12k-p**. Morpholine substituent derivatives (**12k-l**) all exhibited potent anti-tumor activities. However, piperazine substituent derivatives (**12n-p**) reduced inhibitory effects than **12k-l**.

Table 5. IC_{50} values against several cancer cells of compounds **12a-p**, and SAHA as positive control.

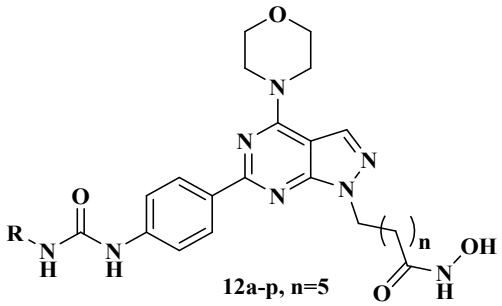

Compd	R	IC_{50} [a] ± SEM, nM		
		HCT116	Raji	MM1S
12a	Me	51.6 ± 30.9	3.5 ± 0.2	13.4 ± 0.3
12b	Et	61.9 ± 2.8	19.7 ± 0.2	11.8 ± 0.4
12c	Pro	103.9 ± 1.9	42.5 ± 1.7	83.4 ± 1.5
12d	*n*-butyl	33.9 ± 0.6	19.1 ± 0.4	15.3 ± 0.4
12e	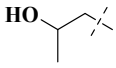	440.7 ± 25.4	152.6 ± 24.9	305.4 ± 21.4
12f	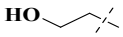	57.2 ± 24.9	61.08 ± 5.9	60.3 ± 9.5
12g	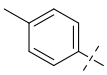	26.1 ± 0.8	22.1 ± 1.2	24.7 ± 0.9
12h		24.6 ± 1.3	19.0 ± 1.4	20.2 ± 1.9
12i	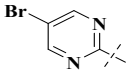	143.5 ± 14.5	60.8 ± 1.3	64.3 ± 4.8
12j	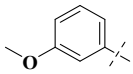	> 500	247.3 ± 95.4	464.3 ± 20.5

12k		100.1 ± 3.1	14.6 ± 0.7	27.8 ± 0.8
12l		17.2 ± 0.3	1.9 ± 0.4	7.3 ± 0.2
12m		68.0 ± 2.0	147.5 ± 3.2	39.2 ± 1.4
12n	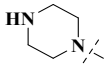	110.9 ± 1.9	127.3 ± 3.3	126.4 ± 3.6
12o	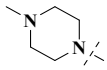	83.5 ± 2.1	70.4 ± 1.8	62.2 ± 3.1
12p	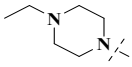	42.9 ± 1.2	34.8 ± 1.4	52.1 ± 2.1
SAHA		882.5 ± 66	196 ± 7	573 ± 9

[a] IC_{50} = compound concentration required to inhibit tumor cell proliferation by 50%; data are expressed as the mean ± SEM from the dose-response curves of at least three independent experiments.

To further evaluate the inhibitory activities of compounds **12b**, **12d**, and **12k-p**, acute myeloid leukemia cells (MV4-11, OCI-AML2, and OCI-AML3) were cultured with these compounds[8, 29]. All these compounds exhibited potent inhibitory activities in these tested cells. Morpholine substituent derivatives (**12k-l**) showed more potent in leukemia cells than other tumor cells with IC_{50} values below 10 nM, equivalent with piperazine substituent derivatives (**12n-p**). However, RAPA (rapamycin) hardly inhibited the three cancer cells and SAHA only showed slight inhibitory effects (IC_{50} > 200 nM).

Table 6. IC_{50} values against leukemia cells of optimal compounds, rapamycin and SAHA as positives.

	IC_{50} [a] ± SEM, nM
Compd	

	MV4-11	OCI-AML2	OCI-AML3
12b	10.38 ± 1.56	18.41 ± 0.04	16.32 ± 1.21
12d	18.32 ± 2.56	9.71 ± 0.38	8.79 ± 0.50
12k	12.64 ± 2.56	28.96 ± 1.92	30.11 ± 2.11
12l	4.05 ± 0.41	9.01 ± 0.53	9.98 ± 0.62
12m	13.87 ± 0.60	16.95 ± 0.03	14.98 ± 1.01
12n	26.53 ± 1.55	32.78 ± 2.28	40.11 ± 2.83
12o	7.01 ± 1.42	8.55 ± 0.46	35.33 ± 2.22
12p	5.86 ± 0.80	3.97 ± 0.27	8.01 ± 0.43
SAHA	220 ± 8	390 ± 11	300 ± 10
RAPA	> 500	> 500	> 500

[a] IC_{50} = compound concentration required to inhibit tumor cell proliferation by 50%; data are expressed as the mean ± SEM from the dose-response curves of at least three independent experiments.

Based on potent inhibition effects in cancer cells, the inhibition effects on mTOR were inevitable to be evaluated to obtain dual target inhibitors. Meanwhile, the morpholinopyrimidine function group was frequently merged in PI3K inhibitors. Thus the selected compounds were evaluated efficacy on mTOR and PI3Kα together. Surprisingly, all the three compounds showed excellent inhibitory activities on mTOR kinase, especially **12l** with IC_{50} of 1.2 nM with improved efficacy > 30 - fold (**10a**, 40 nM). Furthermore, **12l** showed more than 500 - fold selectivity on mTOR inhibition activity vs PI3Kα. **12o** and **12p** showed slightly decreased selectivity on mTOR inhibition activity to PI3Kα.

Table 7. The IC_{50} values on mTOR kinase and inhibition rates on PI3Kα of selected compounds.

Enzyme types		IC_{50} [a], nM		
		12l	**12o**	**12p**
mTOR		1.2	3.4	3.1
PI3Kα, inhibition rate (%)	**1000 nM**	57.3 ± 13.7	98.1 ± 29.6	83.4 ± 8.1
	100 nM	28.3 ± 6.7	52.7 ± 1.8	69.3 ± 7.4

[a] The IC_{50} values and inhibition rates are the means of at least two experiments, with intra- and inter- assay variations of < 10%.

Up to now, **12l** was the optimal potent mTOR inhibitor without PI3Kα inhibition activity, which proved structure modification strategy correctness. The inhibitory activity on HDACs was further evaluated to confirm dual targets on HDACs and mTOR kinase. As shown in Table 4, 7 and 8, **12l** could maintain inhibitory activities on HDACs with improving potency on mTOR. **12l** showed potent inhibitory activities on class I and IIb isoforms with nanomolar or sub-nanomolar IC_{50} values, much more potent than SAHA[30]. Additionally, the IC_{50} values were all > 1000 nM for class IIa and IV isoforms. We can draw conclusion that **12l** indeed was a potent HDAC and mTOR dual target inhibitor.

Table 8. The IC_{50} values on HDACs of compound **12l**, and SAHA as positive control.

Compd	HDACs IC_{50}[a], nM						
	Class I				Class IIb		Class IIa and IV
	1	**2**	**3**	**8**	**6**	**10**	**4, 5, 7, 9, 11**

12l	0.19	0.61	1.47	1.28	1.8	0.58	> 1000
SAHA	11	35	30	172	15	170	> 1000

[a] The IC_{50} values and inhibition rate are the means of at least two experiments, with intra- and inter- assay variations of < 10%.

Kinase Selectivity Profiling. In order to further understand compound **12l**'s selectivity, we then examined its kinome wide selectivity profile with KinaseProfile™ technology by Eurofins Discovery Pharma Services. A panel of 99 related kinases were tested at 1 μM concentration (Table S1). Not surprisingly, **12l** displayed strong binding affinities against mTOR and mTOR/FKBP12. As for the other kinases, especially for PI3K related kinases, **12l** hardly showed inhibitory activities. In conclusion, **12l** didn't inhibit kinases activity except for mTOR kinase.

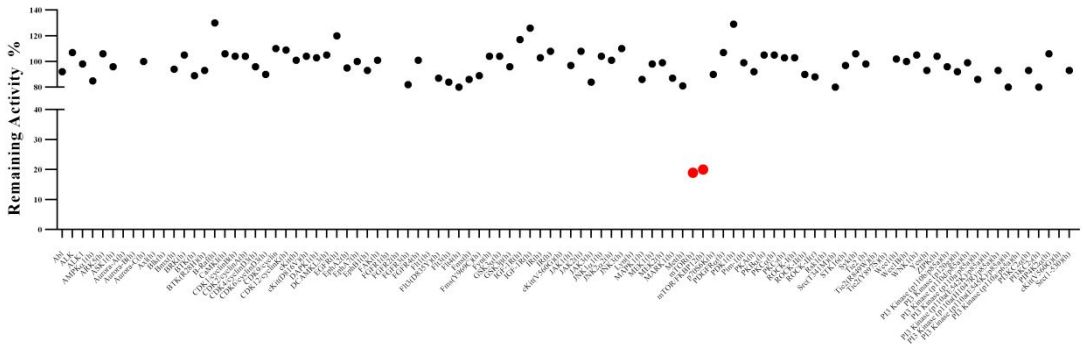

Figure 2. Kinome wide selectivity profiling of compound **12l**. Measurements were performed at a concentration of 1 μM of the inhibitor in duplicate. The % percent control means remaining active kinase percentage. The affinity was defined with respect to a DMSO control.

Molecular Docking Study. To better understand the different activities of **12l** on HDAC1 and mTOR, the molecular docking was performed. The result was shown in

Figure 3A. The hydroxamic tail of **12l** was buried within the narrow active-site channel with the carbonyl oxygen chelating with Zn ion in a similar manner with other class I HDAC inhibitors (for example SAHA bound to HDAC2, PDB code: 4LXZ). The scaffold of pyrazolopyrimidine located at the rim of the HDAC1 active site. In addition, the linking benzene ring formed the π-π stacking with the residues of Phe150 and His28. When aligned the docking pose of **12l** and SAHA in HDAC2 crystal structure, the benzene rings in both structures located at the same position and formed the same contacts with the corresponding residues of Phe and His. The molecular docking with **12l** in mTOR was also performed, and the result was shown in Figure 3B. The docking pose of **12l** could well overlap with the bound PI-103 in mTOR crystal structure. The morpholine ring of **12l** linking to pyrazolopyrimidine made hydrogen bond with Val804 in the hinge region, whereas 4-(*N*-phenylcarbamoyl)-2-methylmorpholine binded to the inner pocket and made hydrogen bond with the residue of Asp759. Moreover, the hydroxamic tail formed three hydrogen bonds with the residues of Thr809, Ala812 and Ser906.

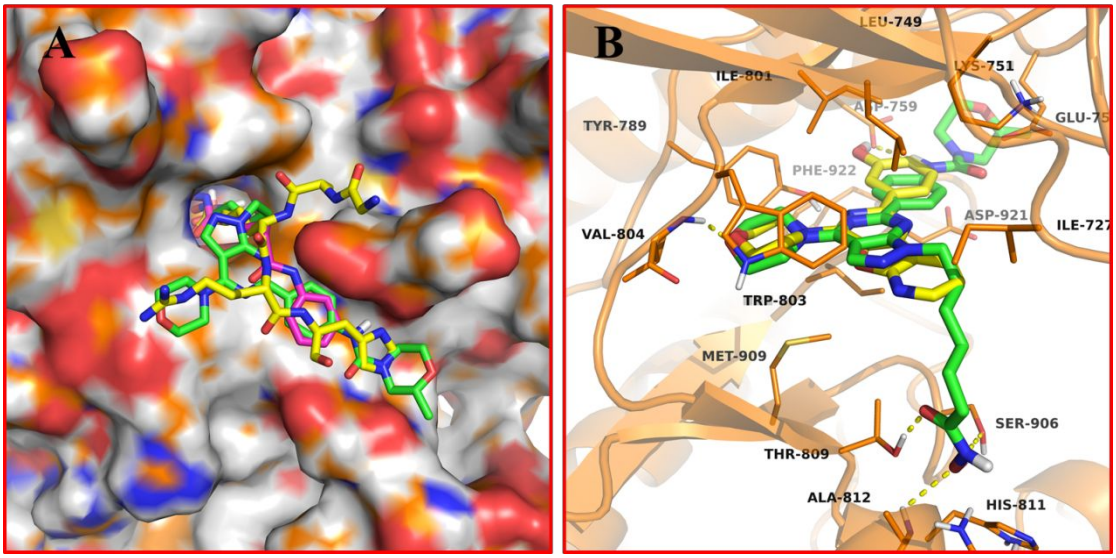

Figure 3. (A) Align the docking pose of **12l** (green stick), the bound peptide inhibitors in HDAC1 (magentas stick, PDB code: 5ICN), and SAHA in HDAC2 (yellow stick, PDB code: 4LXZ); (B) Align the docking pose of **12l** (green stick) and the bound PI-103 in mTOR (yellow stick, PDB code: 4JT6).

Western Blot Confirmed Dual Targets for HDACs and mTOR Kinase. To elucidate signaling pathway inhibition by **12l**, mTOR kinase related upstream and downstream signal factors were detected. As illuminated in Figure 4 (A and C), p-p70S6K (T389) and p-4EBP1 (S65) decreased sharply or even vanished at 0.1 μM, and RAPA showed similar effects only at 1 μM or higher concentration. RAPA induced a rapid and sustained increase in Akt phosphorylation in several types of cancer cells[28, 29], but prolonged RAPA treatment could inhibit mTORC2 assembly and Akt[31], which was consistent with our results. **12l** could blockade phosphorylation of Akt at S473 site at 0.1 μM and higher doses, which resulted from synergistic effects of dual inhibition on HDACs and mTOR kinase[25]. MTORC1 inhibition led to the activation of the extracellular signal-regulated kinase/mitogen-activated protein kinase (ERK/MAPK) cascade in many patients with metastatic cancer[32]. Moreover, RAPA increased p-ERK activity at low concentration while inhibited p-ERK expression at high concentration. **12l** could downregulate p-ERK in a dose-dependent manner from 0.1 to 10 μM, however RAPA decreased p-ERK only at 10 μM. The effects of **12l** on the acetylation level of histone H3 (a known substrate for HDAC 1, 2, and 3) and α-tubulin (a known substrate for HDAC 6), the biomarkers of HDAC inhibition in MV4-11 cells treated with different concentrations were shown in Figure 4 (B). **12l**

induced a concentration-dependent increase of the Ac-H3 from 0.01 μM to 1 μM, however, SAHA only slightly upregulated the Ac-H3 at 1 μM. Furthermore, **12l** concentration-dependently upregulated acetylated α-tubulin, but SAHA induced acetylated α-tubulin increase at slightly higher concentration. Western blot analysis of HDACs indicated that **12l** inhibited HDAC1 more potent than HDAC6 isoform, which was consistent with previous HDACs enzyme assay. These results showed that **12l** was a potent HDACs and mTOR dual target inhibitor.

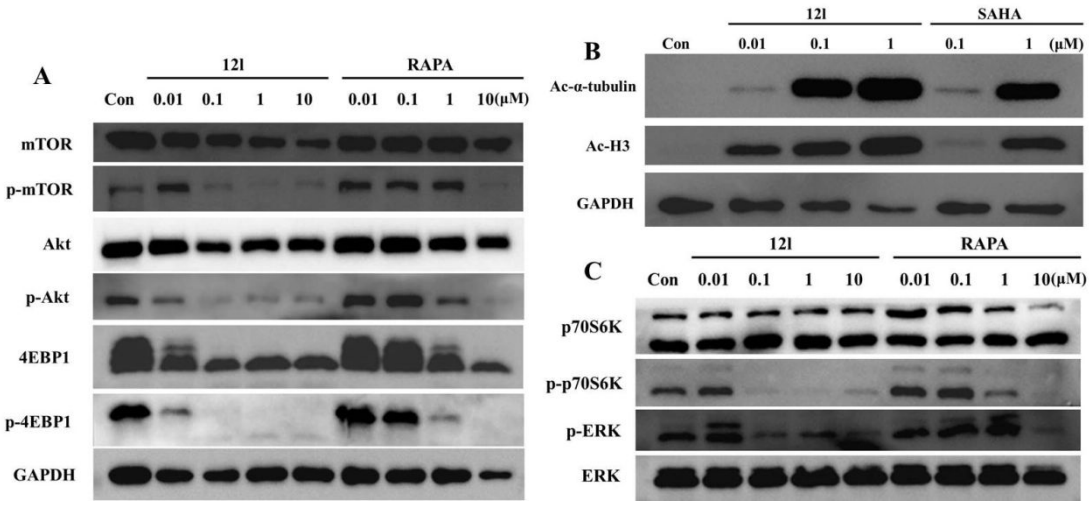

Figure 4. (A, C): MV4-11 cells were treated with **12l** and RAPA for 24 h at 0.01, 0.1, 1, 10 μM, respectively. The cells were harvested for preparation of whole-cell protein lysates and subsequent western blot analysis with the indicated antibodies. (B): Western blot analysis of acetylated α-tubulin, acetylated histone H3 in MV4-11 cells after 6 h treatment with compound **12l**, at 0.01, 0.1, 1 μM and SAHA at 0.1, 1 μM. GAPDH was used as a loading control.

Cell Cycle Analysis and Apoptosis Assays by Flow Cytometry. mTOR is a coordinator of cell fundamental biological processes, which regulates both cell growth and cell cycle progression[33]. Compared to the vehicle, MV4-11 and MM1S cells

treated with **12l** demonstrated a loss of S-phase cells and an increase in the percentage of cells in G_0/G_1 phase (Figure 5A and Figure 6A). We next wanted to confirm that the phenotypic observation of cell death induced by **12l** was specifically due to apoptosis. As shown in Figure 5B and Figure 6B, RAPA (1 μM) alone hardly induced cell apoptosis, and SAHA (1 μM) could induce cell apoptosis. When MV4-11 cells were treated with **12l** at 20 nM, the percentage of the early stage and the later stage of apoptosis was 76.6%, approximatively with SAHA group. Furthermore, the apoptosis effect was consistent as the dose increased. For MM1S cells, the apoptosis effect was stronger as the dose increased. SAHA+RAPA (3:1) group didn't induce stronger apoptosis than SAHA group, indicating inapparent synergistic effects in MV4-11 cells. However, SAHA+RAPA (3:1) group could induce stronger apoptosis than SAHA group, indicating apparent synergistic effects in MM1S cells. It was evident that **12l** blocked the tumor cells in G1-phase progression, which resulted in decreased S-phase populations, and induced tumor cells apoptosis.

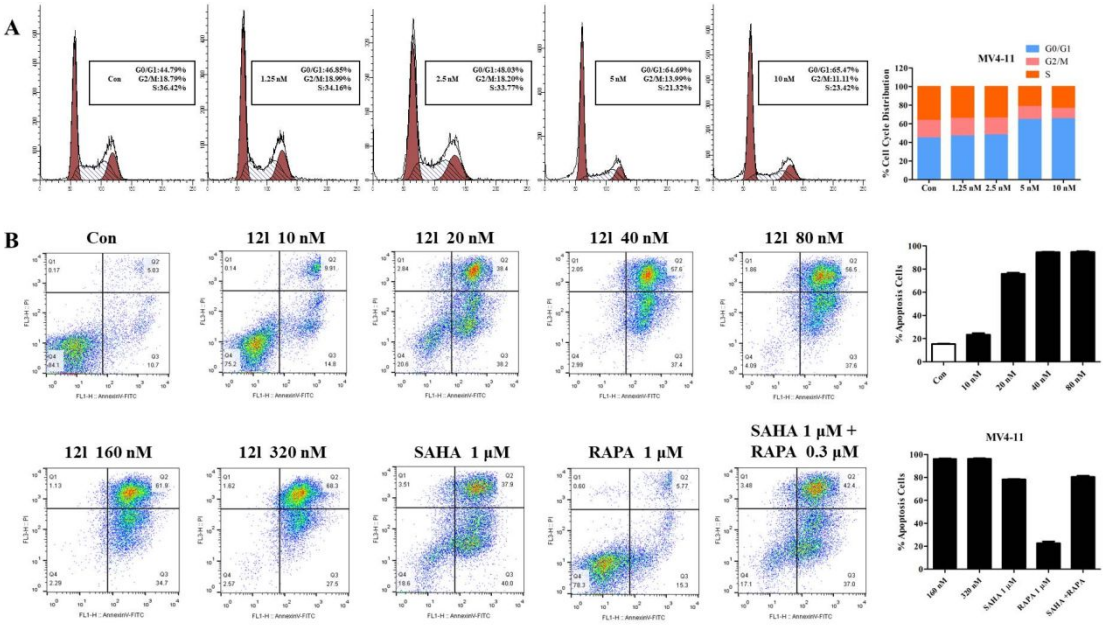

Figure 5. (A): MV4-11 cells were cultured with **12l** from 1.25 to 10 nM for 24 h, the cell cycle distribution of these cells was analyzed. (B): MV4-11 cells were cultured with **12l** from 10 to 1000 nM for 48 h, and SAHA at 1 μM, RAPA at 1 μM, SAHA (1 μM)+RAPA (0.3 μM) were positive controls.

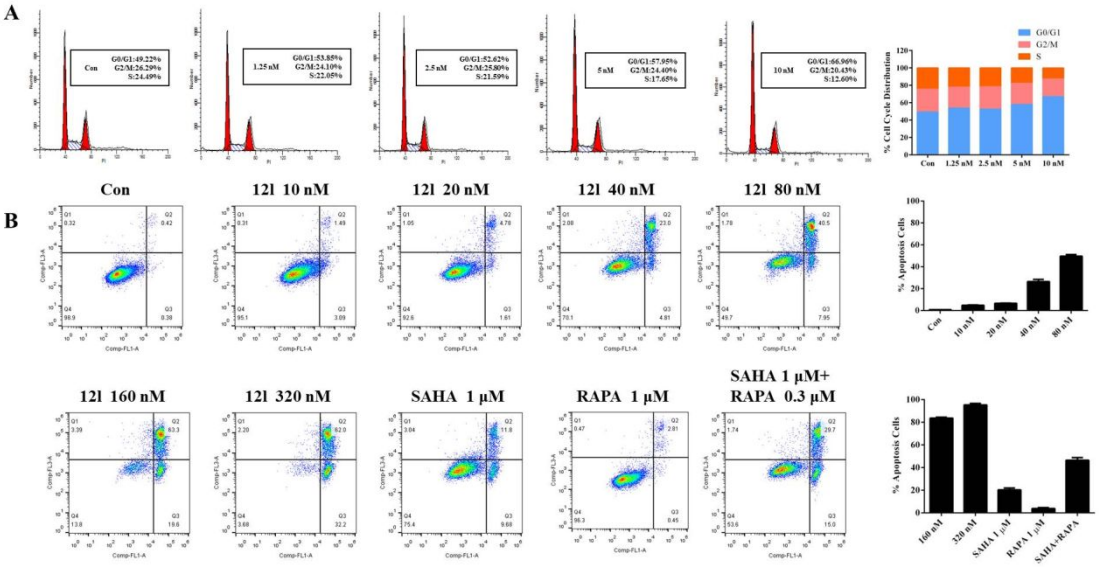

Figure 6. (A): MM1S cells were cultured with **12l** from 1.25 to 10 nM for 24 h, the cell cycle distribution of these cells was analyzed. (B): MM1S cells were cultured with **12l** from 10 to 1000 nM for 48 h, and SAHA at 1 μM, RAPA at 1 μM, SAHA (1 μM)+RAPA (0.3 μM) were positive controls.

In Vivo Xenograft Model Experiments. MV4-11 xenograft NOD/SCID mouse model was primarily established to investigate the efficacy of **12l** in vivo. The administration, dosing schedules, and results were presented in Table 9. **12l** displayed potent anti-tumor effect without significant toxicity: slight body weight change and no death of mice were observed during the treatment period. The TGI (tumor growth inhibitory rate) was up to 53.1%. In order to validate the potent anti-tumor effect due to dual targets for HDACs and mTOR, MM1S model was established subsequently.

SAHA and RAPA were chosen to be double positives. The SAHA group showed a slight anti-tumor efficacy with TGI of 32.5%. As expected, the combination group sharply inhibited tumor growth and TGI was up to 73.8%, which suggested synergistic anti-tumor effects of two target inhibitors, which was consistent with apoptosis effects. The low dosage group of **12l** with 10 mg/kg iv treatment exhibited potent anti-tumor effect and the TGI was 48.1%. The TGI increased to 72.5% after treatment with 20 mg/kg iv of **12l**, which was similar to the combination medication. Conclusion might be drawn that **12l** could exert synergistic effects of dual HDAC and mTOR target inhibitor.

Table 9. Summary of tumor growth inhibition of compound **12l**.

Tumor model	Compd	Administration			Survivors (day)	Tumor mass change(%)
		Schedule[a]	Dose (mg/kg)	Route		
MV4-11	**12l**	Q2D×6	10	iv	6/6	53.1
MM1S	**12l**	Q2D×5	10	iv	6/6	48.1
	12l	Q2D×5	20	iv	6/6	72.5
	SAHA+RAPA	QD×10	50+25	po	6/6	73.8
	SAHA	QD×10	50	po	6/6	32.5

[a] QD, every day; Q2D, every two days.

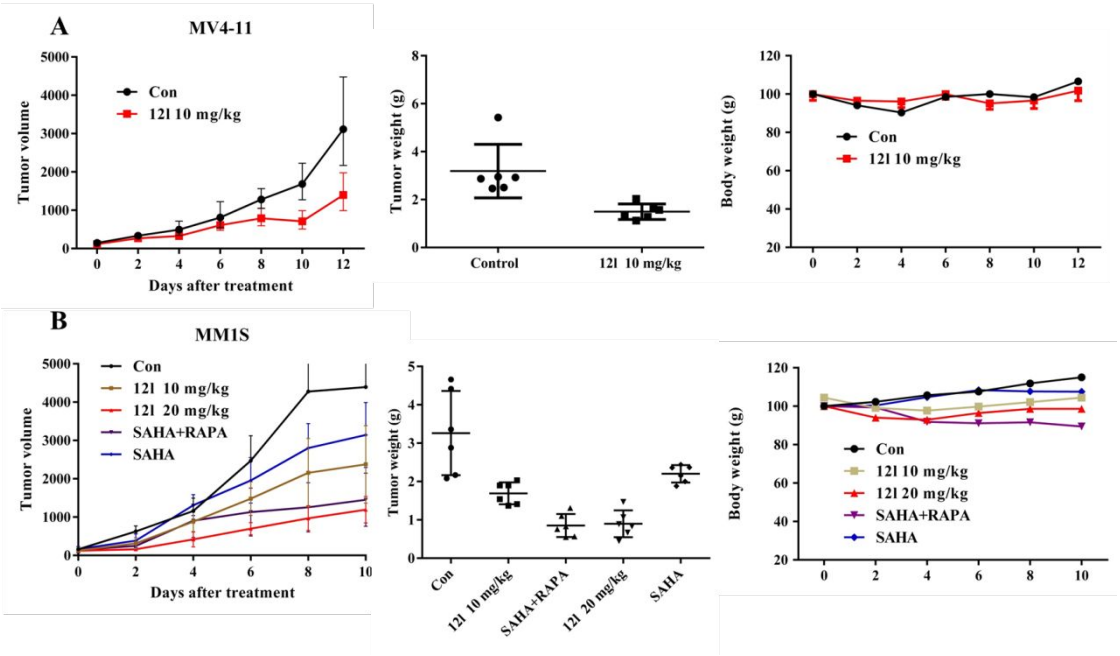

Figure 7. (A): Anti-tumor activity of **12l** in the MV4-11 xenograft model; (B): Anti-tumor activity of **12l** in MM1S xenograft model.

Conclusion

Based on the progress of clinical research of combination of mTOR inhibitors and HDAC inhibitors, our groups decided to design and synthesize dual target inhibitors for mTOR and HDACs. We designed pyrimidine-pyrazolyl pharmacophore to append HDAC recognition cap and hydroxamic acid as a zinc binding motif. Among them, **12l** was the optimal lead compound with potent inhibition for mTOR and HDAC1 with IC_{50} of 1.2 nM and 0.19 nM. Kinome profile confirmed that **12l** hardly hit other kinases except for mTOR. **12l** also showed potent inhibition activities in hematologic malignancies cells, such as MV4-11 and MM1S. Furthermore, western blot confirmed the anti-tumor activities were indeed on-target. **12l** could also stimulate cell cycle arrest in G_0/G_1 phase and induce tumor cell apoptosis. Most importantly, in MM1S xenograft model, **12l** could inhibit tumor growth and the TGI was up to 72.5% at 20

mg/kg iv. In combination medication group, SAHA and RAPA exerted synergistic effects on inhibiting tumor growth. We speculated that the potent anti-tumor activities of **12l** were due to dual target effects. However, the poor bioavailability limited its convenient administration and higher dosage in treating cancers. Thus an optimal formulation may overcome this disadvantage. To sum up, **12l** was a promising dual target inhibitor for treating cancers, especially for hematologic malignancies.

Experimental Section

Chemistry. All the chemical solvents and reagents, which were analytically pure without further purification, were commercially available. TLC was performed on 0.20 mm Silica Gel 60 F_{254} plates (Qingdao Haiyang Chemical, China). ^{1}H NMR and ^{13}C NMR spectra were recorded on a Bruker Avance 400 spectrometer (Bruker Company, Germany) or Varian spectrometer (Varian, Palo Alto, CA), using TMS as an internal standard. Chemical shifts were given in ppm (parts per million). Mass spectra were recorded on Q-TOF Priemier mass spectrometer (Micromass, Manchester, UK). The purity of each compound (> 95%) was determined on an Waters e2695 series LC system (column, Xtimate C18, 4.6 mm ×150 mm, 5 μm; mobile phase, methanol (60%)/H_2O (40%); low rate, 1.0 mL/min; UV wavelength, 254 - 400 nM; temperature, 25 ^{o}C; injection volume, 10 μL).

General Procedures of Method A for the Syntheses of compounds 6a-j.

4-(6-chloro-1*H*-pyrazolo[3,4-*d*]pyrimidin-4-yl)morpholine (**2**). To the mixture of **1** (9.45 g, 50 mmol, 1 equiv) in methanol (250 ml) was added morpholine (6.5 ml, 75 mmol, 1.5 equiv) slowly under ice-bath. The mixture was stirred for 10 min, and

stirred at room temperature for another 2 h. Upon the reaction completed, large amounts of precipitates formed. The precipitates were collected by filtration to get the crude production. Yield, 95%, light yellow power solid. ^{1}H NMR (400 MHz, $CDCl_3$) δ: 10.48 (s, 1H), 7.72 (s, 1H), 3.85 – 3.76 (m, 4H), 3.68 – 3.52 (m, 4H).

4,4'-(*1H*-pyrazolo[3,4-*d*]pyrimidine-4,6-diyl)dimorpholine (**3**). To a solution of **2** (5 g, 17.2 mmol, 1 equiv) in N-methyl pyrrolidone (NMP) (100 ml) was added morphline (7.5 ml, 86 mmol, 5 equiv), *N,N*-diisopropylethylamine (DIEA) (5.7 ml, 34.4 mmol, 2 equiv) and KI (catalytic amount). The vial was sealed under N_2 production and heated with stirring at 90 ^oC for 8 h. The solution was quenched with water and extracted with ethyl acetate. The solvent was removed under reduced pressure to afford the crude **3** without further purification. Yield, 85%. ^{1}H NMR (400 MHz, $CDCl_3$) δ: 10.48 (s, 1H), 7.72 (s, 1H), 3.84 – 3.78 (m, 4H), 3.75 – 3.66 (m, 8H), 3.66 – 3.54 (m, 4H).

4-(6-(4-methylpiperazin-1-yl)-*1H*-pyrazolo[3,4-*d*]pyrimidin-4-yl)morpholine (**4**). Compound **4** could be gotten in similar method with **3**. ^{1}H NMR (400 MHz, $CDCl_3$) δ: 10.50 (s, 1H), 7.79 (s, 1H), 3.95 – 3.79 (m, 12H), 2.61 – 2.48 (s, 4H), 2.39 (s, 3H).

Ethyl-3-(4,6-dimorpholino-*1H*-pyrazolo[3,4-*d*]pyrimidin-1-yl)acidate (**5a-i**). To a mixture of **3** (**4**) in DMF was added Cs_2CO_3, followed by bromoacetate analogues. The mixture was reacted using microwave (MW) at 120 ^oC for 1 h. The mixture was quenched with water and extracted with ethyl acetate. The organic layer was separated and washed with saturated brine. After dried over Na_2SO_4, the solvent was removed

under reduced pressure to afford the crude **5a-g** and **5h-i**. The crude was purified by flash chromatograph as light yellow solid.

(*E*)-methyl-3-(4-((4,6-dimorpholino-*1H*-pyrazolo[3,4-*d*]pyrimidin-1-yl)methyl)ph -enyl)acrylate (**5j**). The intermediate **5j** was gotten in similar synthesis route with methyl 3-(4-bromomethyl)cinnamate instead of bromoacetate analogues. ^{1}H NMR (400 MHz, $CDCl_3$) δ: 7.74 (s, 1H), 7.64 (d, *J* = 16.0 Hz, 1H), 7.45 (d, *J* = 8.2 Hz, 2H), 7.31 (d, *J* = 8.2 Hz, 2H), 6.39 (d, *J* = 16.0 Hz, 1H), 5.44 (s, 2H), 3.89 - 3.85 (m, 4H), 3.85 – 3.80 (m, 8H), 3.79 (s, 3H), 3.78 – 3.74 (m, 4H).

General Procedures of Method A for the Syntheses of Hydroxamic Acid Derivatives. The ester intermediate (1 mmol, 1 equiv) was dissolved in CH_2Cl_2/CH_3OH (10 ml, v:v, 2:1). The resulting solution was cooled to 0 ^oC, then hydroxamic (50 wt % in water, 1 ml, 30 mmol, 30 equiv) and NaOH (400 mg, 10 mmol, 10 equiv) were added. The reaction was stirred for 1 h. The solvent was then removed under reduced pressure, and the obtained solid was dissolved in water, which was adjusted to pH 7-8 by acetic acid and the crude formed in large amounts. After filtration, the crude obtained to yield a solid production which recrystallized with EtOH to give the title compound.

***N*-Hydroxy-2-(4,6-dimorpholino-*1H*-pyrazolo[3,4-*d*]pyrimidin-1-yl)acetamide** (**6a**). **6a** was obtained from compound **5a** as described for method A. ^{1}H NMR (400 MHz, DMSO-d_6) δ: 10.77 (s, 1H), 8.98 (s, 1H), 8.03 (s, 1H), 4.68 (s, 2H), 3.84 – 3.78 (m, 4H), 3.75 – 3.66 (m, 8H), 3.64 (m, 4H). HRMS (ESI), [M+H$^+$] m/z: 364.1746.

***N*-Hydroxy-3-(4,6-dimorpholino-*1H*-pyrazolo[3,4-*d*]pyrimidin-1-yl)propanamide** (**6b**). **6b** was obtained from compound **5b** as described for method A. ^{1}H NMR (400 MHz, DMSO-d_6) δ: 10.47 (s, 1H), 8.76 (s, 1H), 8.00 (s, 1H), 4.33 (t, J = 7.4 Hz, 2H), 3.83 – 3.77 (m, 4H), 3.70 (m, 8H), 3.65 (m, 4H), 2.50 – 2.49 (m, 2H). HRMS (ESI), [M+H$^+$] m/z: 378.1914.

***N*-Hydroxy-4-(4,6-dimorpholino-*1H*-pyrazolo[3,4-*d*]pyrimidin-1-yl)butanamide** (**6c**). **6c** was obtained from compound **5c** as described for method A. ^{1}H NMR (400 MHz, DMSO-d_6) δ: 10.32 (s, 1H), 8.67 (s, 1H), 8.01 (s, 1H), 4.14 (t, J = 6.4 Hz, 2H), 3.84 – 3.77 (m, 4H), 3.74 – 3.66 (m, 8H), 3.65 (m, 4H), 1.94 (m, 4H). HRMS (ESI), [M+H$^+$] m/z: 392.2043.

***N*-Hydroxy-5-(4,6-dimorpholino-*1H*-pyrazolo[3,4-*d*]pyrimidin-1-yl)pentanamide** (**6d**). **6d** was obtained from compound **5d** as described for method A. ^{1}H NMR (400 MHz, DMSO-d_6) δ: 10.31 (s, 1H), 8.64 (s, 1H), 8.00 (s, 1H), 4.13 (t, J = 6.7 Hz, 2H), 3.84 – 3.78 (m, 4H), 3.74 – 3.67 (m, 8H), 3.64 (m, 4H), 1.97 (t, J = 7.3 Hz, 2H), 1.81 – 1.67 (m, 2H), 1.46 – 1.35 (m, 2H). HRMS (ESI), [M+H$^+$] m/z: 406.2186.

***N*-Hydroxy-6-(4,6-dimorpholino-*1H*-pyrazolo[3,4-*d*]pyrimidin-1-yl)hexanamide** (**6e**). **6e** was obtained from compound **5e** as described for method A. ^{1}H NMR (400 MHz, DMSO-d_6) δ: 10.29 (s, 1H), 8.63 (s, 1H), 8.00 (s, 1H), 4.12 (t, J = 6.8 Hz, 2H), 3.84 – 3.78 (m, 4H), 3.74 – 3.66 (m, 8H), 3.64 (m , 4H), 1.90 (t, J = 7.4 Hz, 2H), 1.80 – 1.69 (m, 2H), 1.57 – 1.46 (m, 2H), 1.17 (m, 2H). HRMS (ESI), [M+H$^+$] m/z: 420.2356.

***N*-Hydroxy-7-(4,6-dimorpholino-*1H*-pyrazolo[3,4-*d*]pyrimidin-1-yl)heptanamide** (**6f**). **6f** was obtained from compound **5f** as described for method A. ^{1}H NMR (400 MHz, DMSO-d_6) δ: 10.30 (s, 1H), 8.63 (s, 1H), 8.00 (s, 1H), 4.12 (t, J = 6.8 Hz, 2H), 3.83 – 3.78 (m, 4H), 3.71 (m, 8H), 3.65 (m, 5H), 1.90 (t, J = 7.4 Hz, 2H), 1.74 (p, J = 6.9 Hz, 2H), 1.49 – 1.38 (m, 2H), 1.27 (m, 2H), 1.22 – 1.13 (m, 2H). HRMS (ESI), [M+H$^+$] m/z: 434.2563.

***N*-Hydroxy-8-(4,6-dimorpholino-*1H*-pyrazolo[3,4-*d*]pyrimidin-1-yl)octanamide** (**6g**). **6g** was obtained from compound **5g** as described for method A. ^{1}H NMR (400 MHz, DMSO-d_6) δ: 10.33 (s, 1H), 8.67 (s, 1H), 8.00 (s, 1H), 4.13 (t, J = 6.8 Hz, 2H), 3.84 – 3.78 (m, 4H), 3.74 – 3.67 (m, 8H), 3.65 (m, 4H), 1.91 (t, J = 7.4 Hz, 2H), 1.80 – 1.69 (m, 2H), 1.44 (m, 2H), 1.44 (m, 2H), 1.25 (m, 4H), 1.18 (m, 4H). HRMS (ESI), [M+H$^+$] m/z: 448.2675.

***N*-Hydroxy-6-(6-(4-methylpiperazin-1-yl)-4-morpholino-*1H*-pyrazolo[3,4-*d*]pyrimidin-1-yl)hexanamide** (**6h**). **6h** was obtained from compound **5h** as described for method A. ^{1}H NMR (400 MHz, DMSO-d_6) δ: 10.41 (s, 1H), 8.73 (s, 1H), 8.00 (s, 1H), 4.11 (t, J = 6.2 Hz, 2H), 3.84 – 3.76 (m, 4H), 3.75 – 3.66 (m, 8H), 2.36 – 2.28 (m, 4H), 2.20 (s, 3H), 1.92 (t, J = 6.8 Hz, 2H), 1.79 – 1.69 (m, 2H), 1.59 – 1.42 (m, 2H), 1.21 – 1.10 (m, 2H). HRMS (ESI), [M-H$^+$] m/z: 434.2644.

***N*-Hydroxy-7-(6-(4-methylpiperazin-1-yl)-4-morpholino-*1H*-pyrazolo[3,4-*d*]pyrimidin-1-yl)heptanamide** (**6i**). **6i** was obtained from compound **5i** as described for method A. ^{1}H NMR (400 MHz, DMSO-d_6) δ: 10.32 (s, 1H), 8.63 (s, 1H), 7.98 (s, 1H), 4.12 (t, J = 6.8 Hz, 2H), 3.83 – 3.76 (m, 4H), 3.72 (m, 8H), 2.35 (m, 4H), 2.21 (s,

3H), 1.90 (t, J = 7.3 Hz, 2H), 1.79 – 1.69 (m, 2H), 1.48 – 1.39 (m, 2H), 1.29 - 1.22 (m, 2H), 1.20 – 1.15 (m, 2H). HRMS (ESI), [M+H$^+$] m/z: 447.2854.

***N*-Hydroxy-(*E*)-3-(4-((4,6-dimorpholino-*1H*-pyrazolo[3,4-*d*]pyrimidin-1-yl)methy -l)phenyl)acrylamide (6j)**. **6j** was obtained from compound **5j** as described for method A. ^{1}H NMR (400 MHz, DMSO-d_6) δ: 10.76 (s, 1H), 9.01 (s, 1H), 8.05 (s, 1H), 7.49 (d, J = 8.0 Hz, 2H), 7.40 (d, J = 16.2 Hz, 1H), 7.23 (d, J = 8.2 Hz, 2H), 6.42 (d, J = 15.8 Hz, 1H), 5.37 (s, 2H), 3.81 (m, 4H), 3.71 (m, 8H), 3.64 (m, 4H). HRMS (ESI), [M+H$^+$] m/z: 466.2203.

General Procedures of Method B for the Syntheses of compounds 10a-j.

Ethyl-7-(6-chloro-4-morpholino-*1H*-pyrazolo[3,4-*d*]pyrimidin-1-yl)heptanoate (7). To a mixture of **2** (5 g, 20.87 mmol, 1 equiv) in DMF was added Cs_2CO_3 (13.56 g, 41.74 mmol, 2 equiv), followed by ethyl 7-bromoheptanoate (6.07 ml, 31.3 mmol, 1.5 equiv). The mixture was reacted using microwave (MW) at 120 ^{o}C for 1 h. The mixture was quenched with water and extracted with ethyl acetate. The organic layer was separated and washed with saturated brine. After dried over Na_2SO_4, the solvent was removed under reduced pressure to afford the crude **7**. The crude was purified by flash chromatograph as light yellow solid. Yield, 67%. ^{1}H NMR (400 MHz, $CDCl_3$) δ: 7.90 (s, 1H), 4.34 (t, J = 7.2 Hz, 2H), 4.12 (q, J = 7.2 Hz, 2H), 4.00 – 3.94 (m, 4H), 3.89 – 3.84 (m, 4H), 2.27 (t, J = 7.6 Hz, 2H), 1.94 – 1.85 (m, 2H), 1.65 – 1.55 (m, 2H), 1.41 – 1.28 (m, 4H), 1.25 (t, J = 7.2 Hz, 3H). MS (ESI), [M+H$^+$] m/z: 396.14.

Ethyl-7-(6-R-4-morpholino-*1H*-pyrazolo[3,4-*d*]pyrimidin-1-yl)heptanoate (9a-j). **7** (197.9 mg, 0.5 mmol, 1 equiv) was dissolved in 1,4-dioxane/ethanol/water (v:v:v,

7:3:4, 3 ml) and treated with **8** (0.6 mmol, 1.2 equiv), $PdCl_2$(dppf), and $NaHCO_3$ (84 mg, 1 mmol, 2 equiv). The vial was sealed and heated with stirring at 80 °C for 2 h. The crude reaction mixture was purified by flash chromatograph to afford **9a−j**.

General Procedures of Method B for the Syntheses of Hydroxamic Acid Derivatives. The ester intermediate **9a-j** (1 mmol, 1 equiv) was dissolved in CH_2Cl_2/CH_3OH (10 ml, v:v, 2:1). The resulting solution was cooled to 0 °C, then hydroxamic (50 wt % in water, 1 ml, 30 mmol, 30 equiv) and NaOH (400 mg, 10 mmol, 10 equiv) were added. Th reaction was stirred for 1 h. The solvent was then removed under reduced pressure, and the obtained solid was dissolved in water, which was adjusted to pH 7-8 by acetic acid and the crude formed in large amounts. After filtration, the crude obtained to yield a solid production which recrystallized with EtOH to give the title compound.

***N*-Hydroxy-7-(6-(4-aminophenyl)-4-morpholino-*1H*-pyrazolo[3,4-*d*]pyrimidin-1-yl)heptanamide (10a)**. ^{1}H NMR (400 MHz, DMSO-d_6) δ: 10.30 (s, 1H), 8.63 (s, 1H), 8.20 (s, 1H), 8.15 (d, J = 8.7 Hz, 2H), 6.63 (d, J = 8.7 Hz, 2H), 5.65 (s, 2H), 4.33 (t, J = 6.8 Hz, 2H), 4.00 – 3.92 (m, 4H), 3.81 – 3.74 (m, 4H), 1.91 (t, J = 7.3 Hz, 2H), 1.87 – 1.78 (m, 2H), 1.49 – 1.39 (m, 2H), 1.34 – 1.18 (m, 4H). HRMS (ESI), [M+H$^+$] m/z: 440.2396.

***N*-Hydroxy-7-(6-(2-aminopyrimidin-5-yl)-4-morpholino-*1H*-pyrazolo[3,4-*d*]pyrimidin-1-yl)heptanamide (10b)**. ^{1}H NMR (400 MHz, DMSO-d_6) δ: 9.15 (s, 2H), 8.25 (s, 1H), 7.16 (s, 2H), 4.34 (t, J = 6.4 Hz, 1H), 4.01 - 3.93 (m, 4H), 3.81 - 3.74 (m,

4H), 1.92 (t, *J* = 7.1 Hz, 1H), 1.87 – 1.77 (m, 2H), 1.50 - 1.39 (m, 2H), 1.36 – 1.15 (m, 4H). HRMS (ESI), [M+H $^{+}$] m/z: 441.2345.

***N*-Hydroxy-7-(6-(6-aminopyridin-3-yl)-4-morpholino-*1H*-pyrazolo[3,4-*d*]pyrimid -in-1-yl)heptanamide (10c)**. ^{1}H NMR (400 MHz, DMSO-d_6) δ: 10.32 (s, 1H), 8.97 (d, *J* = 2.0 Hz, 1H), 8.35 (dd, *J* = 8.7, 2.3 Hz, 1H), 8.24 (s, 1H), 6.54 (d, *J* = 8.8 Hz, 1H), 4.34 (t, *J* = 6.8 Hz, 2H), 4.00 - 3.93 (m, 4H), 3.81 – 3.74 (m, 4H), 1.91 (t, *J* = 7.3 Hz, 2H), 1.87 – 1.79 (m, 2H), 1.49 – 1.39 (m, 2H), 1.34 – 1.17 (m, 4H). HRMS (ESI), [M+Na^{+}] m/z: 464.2125.

***N*-Hydroxy-7-(6-(6-methoxypyridin-3-yl)-4-morpholino-*1H*-pyrazolo[3,4-*d*]pyri m-idin-1-yl)heptanamide (10d)**. ^{1}H NMR (400 MHz, DMSO-d_6) δ: 10.30 (s, 1H), 9.20 (d, *J* = 8.7 Hz, 1H), 8.63 (s, 1H), 8.29 (s, 1H), 6.93 (d, *J* = 8.7 Hz, 1H), 4.37 (t, *J* = 6.8 Hz, 2H), 4.00 (m, 4H), 3.93 (s, 3H), 3.82 – 3.75 (m, 4H), 1.91 (t, *J* = 7.3 Hz, 2H), 1.87 – 1.80 (m, 2H), 1.48 – 1.40 (m, 2H), 1.34 – 1.18 (m, 4H). HRMS (ESI), [M+Na^{+}] m/z: 478.2171.

***N*-Hydroxy-7-(6-(4-methoxyphenyl)-4-morpholino-*1H*-pyrazolo[3,4-*d*]pyrimidin-1-yl)heptanamide (10e)**. 1H NMR (400 MHz, DMSO-d_6) δ: 10.31 (s, 1H), 8.62 (s, 1H), 8.38 (d, *J* = 8.9 Hz, 2H), 8.26 (s, 1H), 7.04 (d, *J* = 8.9 Hz, 2H), 4.37 (t, *J* = 6.8 Hz, 2H), 4.02 - 3.96 (m, 4H), 3.83 (s, 3H), 3.81 – 3.76 (m, 4H), 1.91 (t, *J* = 7.3 Hz, 2H), 1.84 (m, 2H), 1.49 – 1.40 (m, 2H), 1.35 – 1.18 (m, 4H). HRMS (ESI), [M+ Na $^{+}$] m/z: 477.2224.

***N*-Hydroxy-7-(4-morpholino-6-(pyridin-3-yl)-*1H*-pyrazolo[3,4-*d*]pyrimidin-1-yl) h-eptanamide (10f)**. ^{1}H NMR (400 MHz, DMSO-d_6) δ: 10.31 (s, 1H), 9.57 (d, *J* = 1.6

Hz, 1H), 8.73 (dt, *J* = 8.0 Hz, 1.6 Hz, 1H), 8.69 (dd, *J* = 4.8, 1.6 Hz, 1H), 8.34 (s, 1H), 7.55 (dd, *J* = 7.9, 4.8 Hz, 1H), 4.41 (t, *J* = 6.8 Hz, 2H), 4.06 – 3.99 (m, 4H), 3.83 – 3.77 (m, 4H), 1.91 (t, *J* = 7.3 Hz, 2H), 1.88 – 1.82 (m, 2H), 1.48 – 1.40 (m, 2H), 1.34 – 1.19 (m, 4H). HRMS (ESI), [M+H $^+$] m/z: 441.2345.

***N*-Hydroxy-7-(6-(4-(methylsulfonyl)phenyl)-4-morpholino-*1H*-pyrazolo[3,4-*d*]pyr-imidin-1-yl)heptanamide (10g)**. ^{1}H NMR (400 MHz, DMSO-d_6) δ: 10.31 (s, 1H), 8.63 (s, 1H), 8.20 (s, 1H), 8.07 (d, *J* = 8.7 Hz, 2H), 7.63 (d, *J* = 8.7 Hz, 2H), 4.33 (t, *J* = 6.8 Hz, 2H), 4.06 – 3.92 (m, 4H), 3.84 – 3.74 (m, 4H), 3.30(s, 3H), 1.91 (t, *J* = 7.3 Hz, 2H), 1.86 – 1.74 (m, 2H), 1.51 – 1.39 (m, 2H), 1.34 – 1.17 (m, 4H). HRMS (ESI), [M+H $^+$] m/z: 503.2445.

***N*-Hydroxy-7-(6-(furan-3-yl)-4-morpholino-*1H*-pyrazolo[3,4-*d*]pyrimidin-1-yl)he-ptanamide (10h)**. ^{1}H NMR (400 MHz, DMSO-d_6) δ: 10.31 (s, 1H), 8.63 (s, 1H), 8.37 (s, 1H), 8.26 (s, 1H), 7.75 (s, 1H), 7.03 (s, 1H), 4.32 (t, *J* = 6.8 Hz, 2H), 4.00 - 3.92 (m, 4H), 3.80 - 3.74 (m, 4H), 1.91 (t, *J* = 7.2 Hz, 2H), 1.87 – 1.78 (m, 2H), 1.49 – 1.39 (m, 2H), 1.34 – 1.16 (m, 4H). HRMS (ESI), [M+ Na $^+$] m/z: 437.1904.

***N*-Hydroxy-7-(4-morpholino-6-(1H-pyrrol-3-yl)-*1H*-pyrazolo[3,4-*d*]pyrimidin-1-yl)heptanamide (10i)**. ^{1}H NMR (400 MHz, DMSO-d_6) δ: 11.36 (s, 1H), 10.31 (s, 1H), 8.65 (s, 1H), 8.19 (s, 1H), 6.92 (dd, *J* = 2.4, 1.6 Hz, 1H), 6.87 (dt, *J* = 2.0, 1.6 Hz, 1H), 6.15 (dd, *J* = 2.0, 1.6 Hz, 1H), 4.31 (t, *J* = 6.9 Hz, 2H), 4.02 - 3.95 (m, 4H), 3.80 – 3.73 (m, 4H), 1.91 (t, *J* = 7.3 Hz, 2H), 1.86 – 1.77 (m, 2H), 1.50 – 1.39 (m, 2H), 1.34 – 1.17 (m, 4H). HRMS (ESI), [M+ Na $^+$] m/z: 436.2224.

***N*-Hydroxy-7-(4-morpholino-6-(thiophen-3-yl)-*1H*-pyrazolo[3,4-*d*]pyrimidin-1-yl)heptanamide (10j)**. ^{1}H NMR (400 MHz, DMSO-d_6) δ: 10.31 (s, 1H), 9.57 (d, J = 1.6 Hz, 1H), 8.73 (d, J = 8.0 Hz, 1H), 8.69 (dd, J = 4.8, 1.6 Hz, 1H), 8.34 (s, 1H), 7.55 (dd, J = 7.9, 4.8 Hz, 1H), 4.41 (t, J = 6.8 Hz, 2H), 4.06 – 3.99 (m, 4H), 3.83 – 3.75 (m, 4H), 1.91 (t, J = 7.3 Hz, 2H), 1.88 – 1.81 (m, 2H), 1.49 – 1.40 (m, 2H), 1.34 – 1.19 (m, 4H). HRMS (ESI), [M+ Na^+] m/z: 453.2599.

General Procedures of Method C for Formation of Urea. To a solution of aniline **9a** (200 mg, 0.442 mmol, 1 equiv) in CH_2Cl_2 was added TEA (124 μL) and triphosgene (79.5 mg, 0.265 mmol, 0.6 equiv). The mixture was stirred for 15 min at room temperature and was then added to a solution of RNH or RNH_2 in CH_2Cl_2. After reaction for 30 min, the solvents were evaporated and the crude was purified by flash chromatograph to get **11a-p** as white solid.

The uera intermediate **11a-p** (0.3 mmol, 1 equiv) was dissolved in CH_2Cl_2/CH_3OH (6 ml, v:v, 2:1). The resulting solution was cooled to 0 ^oC, then hydroxamic (50 wt % in water, 0.3 ml, 3 mmol, 30 equiv) and NaOH (120 mg, 3 mmol, 10 equiv) were added. Th reaction was stirred for 1 h. The solvent was then removed under reduced pressure, and the obtained solid was dissolved in water, which was adjusted to pH 7-8 by acetic acid and the crude formed in large amounts. After filtration, the crude obtained to yield a solid production which recrystallized with EtOH to give the title compound (**12a-p**).

***N*-Hydroxy-7-(6-(4-(3-methylureido)phenyl)-4-morpholino-*1H*-pyrazolo[3,4-*d*]pyr-imidin-1-yl)heptanamide (12a)**. ^{1}H NMR (400 MHz, DMSO-d_6) δ: 9.20 (s, 1H),

8.30 (d, *J* = 8.7 Hz, 2H), 8.25 (s, 1H), 7.54 (d, *J* = 8.6 Hz, 2H), 6.57 (m, 1H), 4.36 (t, *J* = 6.7 Hz, 2H), 4.03 - 3.94 (m, 4H), 3.82 - 3.75 (m, 4H), 2.66 (d, *J* = 4.2 Hz, 3H), 1.92 (t, *J* = 7.3 Hz, 2H), 1.88 – 1.78 (m, 2H), 1.50 - 1.40 (m, 2H), 1.36 – 1.17 (m, 4H). MS (ESI), [M+H $^+$] m/z: 497.65.

***N*-Hydroxy-7-(6-(4-(3-ethylureido)phenyl)-4-morpholino-*1H*-pyrazolo[3,4-*d*]pyri-midin-1-yl)-heptanamide (12b)**. ^{1}H NMR (400 MHz, DMSO-d_6) δ :10.35 (s, 1H), 9.32 (s, 1H), 8.30 (d, *J* = 8.7 Hz, 2H), 8.25 (s, 1H), 7.54 (d, *J* = 8.6 Hz, 2H), 6.87 (t, *J* = 6.4 Hz, 1H), 4.36 (t, *J* = 6.7 Hz, 2H), 4.02 - 3.95 (m, 4H), 3.82 - 3.75 (m, 4H), 3.17 – 3.07 (qui, *J* = 6.4, 7.2 Hz, 2H), 1.91 (q, *J* = 7.1 Hz, 2H), 1.88 - 1.80 (m, 2H), 1.51 – 1.40 (m, 2H), 1.35 – 1.19 (m, 4H), 1.06 (t, *J* = 7.1 Hz, 3H). MS (ESI), [M+H $^+$] m/z: 511.60.

***N*-Hydroxy-7-(4-morpholino-6-(4-(3-propylureido)phenyl)-*1H*-pyrazolo[3,4-*d*]py-rimidin-1-yl)heptanamide (12c)**. ^{1}H NMR (400 MHz, DMSO-d_6) δ: 10.36 (s, 1H), 9.15 (s, 1H), 8.64 (s, 1H), 8.30 (d, *J* = 8.7 Hz, 2H), 8.25 (s, 1H), 7.51 (d, *J* = 8.6 Hz, 2H), 6.61-6.56 (m, 1H), 4.37 (t, *J* = 6.6 Hz, 2H), 4.04-3.95 (m, 4H), 3.82-3.76 (m, 4H), 3.06 (dd, *J* = 12.7, 6.5 Hz, 2H), 1.92 (t, *J* = 7.3 Hz, 2H), 1.86 (dd, *J* = 13.6, 6.8 Hz, 2H), 1.50-1.40 (m, 4H), 1.37 – 1.18 (m, 4H), 0.89 (t, *J* = 7.4 Hz, 3H). MS (ESI), [M+H $^+$] m/z: 525.66.

***N*-Hydroxy-7-(6-(4-(3-butylureido)phenyl)-4-morpholino-*1H*-pyrazolo[3,4-*d*]pyri-midin-1-yl)heptanamide (12d)**. ^{1}H NMR (400 MHz, DMSO-d_6) δ: 10.34 (s, 1H), 8.81 (s, 1H), 8.65 (s, 1H), 8.31 (d, *J* = 8.6 Hz, 2H), 8.25 (s, 1H), 7.51 (d, *J* = 8.6 Hz, 2H), 6.31 (t, *J* = 5.1 Hz, 1H), 4.37 (t, *J* = 6.7 Hz, 2H), 3.99 (m, 4H), 3.80 (m, 4H),

3.10 (dd, *J* = 12.5, 6.4 Hz, 2H), 1.91 (t, *J* = 7.3 Hz, 2H), 1.88 – 1.79 (m, 2H), 1.50 – 1.38 (m, 4H), 1.38 – 1.18 (m, 6H), 0.91 (t, *J* = 7.2 Hz, 3H). MS (ESI), [M+K $^+$] m/z: 577.26.

***N*-Hydroxy-7-(6-(4-(3-(2-hydroxypropyl)ureido)phenyl)-4-morpholino-*1H*-pyrazolo[3,4-*d*]pyrimidin-1-yl)heptanamide (12e)**. ^{1}H NMR (400 MHz, DMSO-d_6) δ: 9.32 (s, 1H), 8.30 (d, *J* = 7.5 Hz, 2H), 8.25 (s, 1H), 7.52 (d, *J* = 6.2 Hz, 2H), 6.69 (s, 1H), 4.36 (m, 2H), 3.99 (m, 4H), 3.79 (m, 4H), 3.68 (m, 1H), 3.12 (m, 1H), 3.00 (m, 1H), 1.97 – 1.77 (m, 4H), 1.50-1.42 (m, 2H), 1.35-1.17 (m, 4H), 1.07 (d, *J* = 5.3 Hz, 3H). MS (ESI), [M+H $^+$] m/z: 541.64.

***N*-Hydroxy-7-(6-(4-(3-(2-hydroxyethyl)ureido)phenyl)-4-morpholino-*1H*-pyrazolo[3,4-*d*]pyrimidin-1-yl)heptanamide (12f)**. ^{1}H NMR (400 MHz, DMSO-d_6) δ: 10.34 (s, 1H), 8.83 (s, 1H), 8.62 (s, 1H), 8.31 (d, *J* = 8.4 Hz, 2H), 8.25 (s, 1H), 7.50 (d, *J* = 8.3 Hz, 2H), 6.28 (s, 1H), 4.77-4.72 (m, 1H), 4.36 (t, *J* = 6.5 Hz, 2H), 3.99 (s, 4H), 3.79 (s, 4H), 3.46 (d, *J* = 5.0 Hz, 2H), 3.18 (d, *J* = 5.2 Hz, 2H), 1.96 – 1.79 (m, 4H), 1.49-1.40 (m, 2H), 1.34-1.18 (s, 4H). MS (ESI), [M+H $^+$] m/z: 527.62.

***N*-Hydroxy-7-(4-morpholino-6-(4-(3-(p-tolyl)ureido)phenyl)-*1H*-pyrazolo[3,4-*d*]p-yrimidin-1-yl)heptanamide (12g)**. ^{1}H NMR (400 MHz, DMSO-d_6) δ: 10.31 (s, 1H), 9.07 (s, 1H), 8.81 (s, 1H), 8.36 (d, *J* = 8.5 Hz, 2H), 8.26 (s, 1H), 7.58 (d, *J* = 8.4 Hz, 2H), 7.37 (d, *J* = 8.1 Hz, 2H), 7.10 (d, *J* = 8.1 Hz, 2H), 4.38 (t, *J* = 6.6 Hz, 2H), 4.00 (s, 4H), 3.80 (m, 4H), 2.25 (s, 3H), 1.92 (t, *J* = 7.3 Hz, 2H), 1.88 – 1.80 (m, 2H), 1.45 (m, 2H), 1.39 – 1.19 (m, 4H). MS (ESI), [M+H $^+$] m/z: 573.68.

***N*-Hydroxy-7-(6-(4-(3-(3-methylpyridin-2-yl)ureido)phenyl)-4-morpholino-*1H*-py-razolo[3,4-*d*]pyrimidin-1-yl)heptanamide (12h)**. ^{1}H NMR (400 MHz, DMSO-d_6) δ: 11.86 (s, 1H), 10.38 (s, 1H), 8.41 (d, J = 8.1 Hz, 2H), 8.27 (d, J = 8.8 Hz, 2H), 7.74-7.66 (m, 3H), 7.09-7.04 (m, 1H), 4.44-4.34 (m, 2H), 4.06-3.97 (m, 4H), 3.85-3.76 (m, 4H), 2.32 (s, 3H), 2.04 – 1.79 (m, 4H), 1.52-1.41 (m, 2H), 1.38-1.18 (m, 4H). MS (ESI), [M+H$^+$] m/z: 574.63.

***N*-Hydroxy-7-(6-(4-(3-(5-bromopyrimidin-2-yl)ureido)phenyl)-4-morpholino-*1H*-pyrazolo[3,4-*d*]pyrimidin-1-yl)-heptanamide (12i)**. ^{1}H NMR (400 MHz, DMSO-d_6) δ: 10.50 (s, 1H), 9.85 (s, 1H), 8.78(s, 2H), 8.40 (d, J = 7.6 Hz, 2H), 8.25 (s, 1H), 7.52 (d, J = 7.2 Hz, 2H), 4.37-4.34 (m, 2H), 4.03-3.97 (m, 4H), 3.83-3.79 (m, 4H), 1.92 (t, J = 7.3 Hz, 2H), 1.88 – 1.78 (m, 2H), 1.50 - 1.40 (m, 2H), 1.36 – 1.17 (m, 4H). MS (ESI), [M+Na$^+$] m/z: 662.24.

***N*-Hydroxy-7-(6-(4-(3-(3-methoxyphenyl)ureido)phenyl)-4-morpholino-*1H*-pyraz-olo[3,4-*d*]pyrimidin-1-yl)heptanamide (12j)**. ^{1}H NMR (400 MHz, DMSO-d_6) δ: 8.36 (d, J = 6.2 Hz, 1H), 8.26 (s, 1H), 7.62 (d, J = 6.2 Hz, 2H), 7.26 (s, 1H), 7.20 - 7.16 (s, 1H), 7.02 (s, 1H), 6.57 - 6.5 (m, 1H), 4.43 - 4.33 (m, 2H), 4.00 (s, 4H), 3.85-3.69 (m, 7H), 2.27-2.07 (m, 2H), 1.93-1.81 (m, 2H), 1.56-1.44 (m, 2H), 1.41-1.17 (m, 4H). MS (ESI), [M+H$^+$] m/z: 589.67.

***N*-(4-(1-(7-(hydroxyamino)-7-oxoheptyl)-4-morpholino-*1H*-pyrazolo[3,4-*d*]pyrimi-din-6-yl)phenyl)morpholine-4-carboxamide (12k)**. ^{1}H NMR (400 MHz, DMSO-d_6) δ: 10.31 (s, 1H), 8.77 (s, 1H), 8.64 (s, 1H), 8.33 (d, J = 8.7 Hz, 2H), 8.26 (s, 1H), 7.60 (d, J = 8.7 Hz, 2H), 4.37 (t, J = 6.7 Hz, 2H), 4.00 (m, 4H), 3.80 (m, 4H),

3.67 – 3.58 (m, 4H), 3.51 – 3.42 (m, 4H), 1.91 (t, *J* = 7.3 Hz, 2H), 1.88 – 1.79 (m, 2H), 1.44 (dd, *J* = 14.4, 7.1 Hz, 2H), 1.35 – 1.17 (m, 4H). MS (ESI), [M+H $^+$] m/z: 553.31.

(*R*)-*N*-(4-(1-(7-(hydroxyamino)-7-oxoheptyl)-4-morpholino-*1H*-pyrazolo[3,4-*d*]py-rimidin-6-yl)phenyl)-2-methylmorpholine-4-carboxamide (**12l**). ^{1}H NMR (400 MHz, DMSO-d_6) δ: 10.31 (s, 1H), 8.75 (s, 1H), 8.63 (s, 1H), 8.32 (d, *J* = 8.8 Hz, 2H), 8.26 (s, 1H), 7.59 (d, *J* = 8.7 Hz, 2H), 4.37 (t, *J* = 6.7 Hz, 2H), 4.06 – 3.92 (m, 6H), 3.89 – 3.74 (m, 5H), 3.53 – 3.42 (m, 2H), 2.89 (td, *J* = 12.9, 3.2 Hz, 1H), 2.62 – 2.52 (m, 1H), 1.91 (t, *J* = 7.3 Hz, 2H), 1.87 – 1.80 (m, 2H), 1.44 (dd, *J* = 14.5, 7.2 Hz, 2H), 1.35 – 1.18 (m, 4H), 1.13 (d, *J* = 6.2 Hz, 3H). MS (ESI), [M+H $^+$] m/z: 567.30.

***N*-(4-(1-(7-(hydroxyamino)-7-oxoheptyl)-4-morpholino-*1H*-pyrazolo[3,4-*d*]pyrimi-din-6-yl)phenyl)thiomorpholine-4-carboxamide** (**12m**). ^{1}H NMR (400 MHz, DMSO-d_6) δ: 10.36 (s, 1H), 8.83 (s, 1H), 8.32 (d, *J* = 8.6 Hz, 2H), 8.27 (s, 1H), 7.61 (d, *J* = 8.5 Hz, 2H), 4.37 (t, *J* = 6.4 Hz, 2H), 4.00 (m, 4H), 3.78 (m, 8H), 2.62 (m, 4H), 1.92 (t, *J* = 7.2 Hz, 2H), 1.88 – 1.80 (m, 2H), 1.52 – 1.38 (m, 2H), 1.36 – 1.16 (m, 4H). MS (ESI), [M+H $^+$] m/z: 569.27.

***N*-(4-(1-(7-(hydroxyamino)-7-oxoheptyl)-4-morpholino-*1H*-pyrazolo[3,4-*d*]pyrimi-din-6-yl)phenyl)piperazine-1-carboxamide** (**12n**). ^{1}H NMR (400 MHz, DMSO-d_6) δ: 10.36 (s, 1H), 8.93 (s, 1H), 8.34 (d, *J* = 8.4 Hz, 2H), 8.27 (s, 1H), 7.65 (d, *J* = 8.6 Hz, 2H), 4.38 (t, *J* = 6.4 Hz, 2H), 4.00 (m, 4H), 3.80 (m, 4H), 3.58 (m, 4H), 3.44 (m, 4H), 1.92 (t, *J* = 7.1 Hz, 2H), 1.89 – 1.79 (m, 2H), 1.51 – 1.39 (m, 2H), 1.36 – 1.17 (m, 4H). MS (ESI), [M+H $^+$] m/z: 552.31.

***N*-(4-(1-(7-(hydroxyamino)-7-oxoheptyl)-4-morpholino-*1H*-pyrazolo[3,4-*d*]pyrimi -din-6-yl)phenyl)-4-methylpiperazine-1-carboxamide (12o)** ^{1}H NMR (400 MHz, DMSO-d_6) δ: 10.30 (s, 1H), 8.72 (s, 1H), 8.62 (s, 1H), 8.31 (d, *J* = 8.7 Hz, 2H), 8.26 (s, 1H), 7.59 (d, *J* = 8.7 Hz, 2H), 4.37 (t, *J* = 6.7 Hz, 2H), 4.00 (m, 4H), 3.82 - 3.76 (m, 4H), 3.51 – 3.41 (m, 4H), 2.38 – 2.28 (m, 4H), 2.21 (s, 3H), 1.91 (t, *J* = 7.3 Hz, 2H), 1.87 – 1.79 (m, 2H), 1.44 (dd, *J* = 14.5, 7.2 Hz, 2H), 1.36 – 1.17 (m, 4H). MS (ESI), [M+H$^+$] m/z: 566.32.

***N*-(4-(1-(7-(hydroxyamino)-7-oxoheptyl)-4-morpholino-1H-pyrazolo[3,4-*d*]pyrimi -din-6-yl)phenyl)-4-ethylpiperazine-1-carboxamide (12p)**. ^{1}H NMR (400 MHz, DMSO-d_6) δ: 10.31 (s, 1H), 8.74 (s, 1H), 8.32 (d, *J* = 8.6 Hz, 2H), 8.26 (s, 1H), 7.60 (d, *J* = 8.6 Hz, 2H), 4.37 (t, *J* = 6.5 Hz, 2H), 4.00 (m, 4H), 3.79 (m, 4H), 3.47 (m, 4H), 2.40-2.29 (m, 6H), 1.91 (t, *J* = 7.2 Hz, 2H), 1.88 – 1.79 (m, 2H), 1.51 – 1.39 (m, 2H), 1.35 – 1.16 (m, 4H), 1.03 (t, *J* = 7.1 Hz, 3H). MS (ESI), [M+H$^+$] m/z: 581.32. MS (ESI), [M+H$^+$] m/z: 580.34.

Biological Assay Methods

Anti-proliferative Assays. HCT116 and MCF-7 cells were cultured in DMEM (Gibco, Milano, Italy) contained 10% fetal bovine serum (FBS) (Invitrogen, Milano, Italy). MM1S, Ramos, and Raji cells were cultured in RPMI 1640 (Gibco, Milano, Italy) containing 10% fetal bovine serum (FBS) (Invitrogen, Milano, Italy). MV4-11, OCI-AML2, and OCI-AML3 cells were cultured in IMDM (Gibco, Milano, Italy) contained 10% fetal bovine serum (FBS) (Invitrogen, Milano, Italy). All media contained 100 units/mL penicillin (Gibco, Milano, Italy), and 100 μg/mL

streptomycin (Gibco, Milano, Italy). Cells were incubated at 37 ^{o}C in a humidified atmosphere of 5% CO_2. Cells in logarithmic phase were seeded into 96-well culture plates at densities of (10000-15000) cells per well. After 24 h, cells were treated with various concentrations of compounds for 72 h in final volumes of 200 μL. Upon end point, 20 μL MTT (5 mg/mL) was added to each well, and the cells were incubated for an additional 1-3 h. After treatment with 20% SDS overnight, absorbance values at a wavelength of 570 nM were taken on a spectrophotometer (Molecular Devices, Sunnyvale, USA). IC_{50} values were calculated using percentage of growth versus untreated control.

PI3Kα Inhibition Assays. The PI3K activity assay was performed by Chempartner company (Shanghai, China). Enzyme (PI3Kα (p110α/p85a) from Invitrogen, PIP2 (life technologies) substrate and ATP (Sigma) in kinase buffer to the indicated concentrations, covered the assay plate and incubated at room temperature (PI3Kα, 1 h,). Then added the Kinase-Glo reagent (Promega) and incubated for 15 min in PI3Kα inhibition Assay. Collect data on Flex station. Data was presented in MS Excel and the curves fitted by GraphPad Prism V5.0.

mTOR Inhibition Assays. In vitro mTOR inhibition assay was produced by Chempartner company (Shanghai, China). In the assay, diluted the mTOR enzyme (Millipore), ATP (Sigma), the compounds, and Ulight-4E-BP1 (Thr37/46) Peptide (PE) in Kinase Buffer to the indicated concentrations, covered the assay plate and incubated the enzymatic reaction at room temperature for 1 h. After that, added the detection solution buffer, which contained the indicated concentrations of kinase

quench buffer (EDTA) and Eu-anti-phospho-4E-BP1 antibody, covered the mixture and allowed the plate to equilibrate for 1 h at room temperature. Read signal with the EnVision® Multilabel Reader in TR-FRET mode (excitation at 320 or 340 nm and emission at 665 nm). Data was presented in MS Excel and the curves fitted by GraphPad Prism V5.0.

HDAC Enzymes Inhibition Assays. The HDAC activity of compounds **10a** and **12l** in vitro were performed by Chempartner company (Shanghai, China) with fluorigenic release of 7-amino-4-methylcoumarin (AMC) from substrate upon deacetylase enzymatic activity. Briefly, the release of AMC was promoted in the existence of trypsin. The compounds, diluted to the indicated concentrations, with full-length recombinant HDAC enzymes (BPS Biosciences), incubated at room temperature for 15 min, then followed by adding trypsin as well as Ac-peptide-AMC substrates, and the mixture was incubated at room temperature for 1 h. Reactions were performed in Tris-based assay buffer. The fluorescence measurements were obtained using a multilabel plate reader with excitation at 355 nm and emission at 460 nm. Data were analyzed on a plate-by-plate basis for the linear range of fluorescence over time. Wells containing recombinant HDAC, substrate and trypsin in the absence of small molecular inhibitors were set as control wells. Thus the data acquired from the groups containing the tested compounds were referred to the control wells. All of the designed groups, including controls, were run in duplicate. The data were finally fitted in GraphPad Prism V5.0 software to obtain IC_{50} values using equation (Y=Bottom +

(Top-Bottom)/(1+10^((LogIC50-X)*Hill Slope), Y is % inhibition and X is compound concentration).

Kinase Profile Assay. Kinase profiling was carried out by Eurofins Discovery Pharma Services UK Limited according to the published protocols. The kinases activity of 1 μM **12l** on 99 kinases involved in tumor regulation in vitro were measured by radiometric assays. Briefly, each kinase was incubated with 1 μM **12l** in indicated reaction solutions contained [γ-^{33}P-ATP] and other reagents such as MOPS, EDTA, EAIYAAPFAKKK, Magnesium acetate and so on (different pH, concentrations and activities according to the specific needs of different kinases). The reaction is initiated by the addition of the Mg(n)/ATP mix. After incubation for a while (specific time as required) at room temperature, the reaction is stopped by the addition of phosphoric acid to a concentration of 0.5%. 10 μL of the stopped reaction is spotted onto a P30 filtermat and washed four times for 4 minutes in 0.425% phosphoric acid and once in methanol prior to drying and scintillation counting.

Molecular Docking Study

In order to understand the potential binding modes of **12l** in HDAC1 and mTOR, we performed the molecular docking by the GOLD5.0 software. For HDAC1, We used the crystal structure reported by Peter J. Watson (PDB: 5ICN)[34]. And the structure of human HDAC2 in complex with SAHA (PDB: 4LXZ)[35] was used to compare with the docking results. For mTOR, the crystal structure of 4JT6[36] was used and the only kinase domain was retained. In the process of docking, the binding site was set 7.5 Å,

and the Goldscore scoring function was used. The other docking parameters were set as default value.

Western Blotting. The cells were treated with the compounds at the indicated concentrations. Then the cells were collected and total proteins were extracted with RIPA Lysis Buffer (beyotime Co. P0013B, components: 50 mM Tris, pH 7.4, 150 mM NaCl, 1% Triton X-100, 1% sodium deoxycholate, 0.1% SDS, 1 mM sodium orthovanadate, sodium fluoride, EDTA and leupeptin). The protein concentration was measured by the BCA Protein assay (ThermoScientific, USA). Equivalent samples (30 μg of protein) were subjected to SDS-PAGE, and then the proteins were transferred onto PVDF membranes (Millipore, USA). After blocking by 5% non-fat milk for 1 h at room temperature, the membranes were incubated with the indicated primary antibodies at 4 ^{o}C overnight and subsequently probed by the appropriate secondary antibodies conjugated to horseradish peroxidase for 1 h. Immunoreactive bands were visualized using enhanced chemiluminescence (Millipore, USA). The molecular sizes of the proteins detected were determined by comparison with pertained protein markers (ThermoScientific, USA).

Cell Cycle Progression Experiment. Six-well plates were used for MV4-11 and MM1S cells culture. All cells were treated with increasing concentrations of the indicated compounds. Cells were harvested 24 h post-treatment, washed in phosphate buffered saline (PBS), and fixed in ice cold 75% ethanol for at least 24 h. The fixed cells were then washed with room temperature PBS and stained with propidium iodide (50 mg/mL) in the presence of RNase A (0.5 mg) for 30 min at 37 °C. The

stained cells were then analyzed using a FACSCAN (BD Biosciences) and the resulting data analyzed with cell cycle analysis software (Modfit, BD).

Annexin V-FITC/PI Apoptosis Assay. Six-well plates were used for cells culture. MV4-11 and MM1S cells were treated with **12l** at 2-fold gradient increase from 10 to 320 nM, SAHA (1 μM) , RAPA (1 μM), and SAHA (1 μM)+RAPA (0.3 μM) for 48 h. Cells were washed with PBS for twice and collected to stain with an Annexin V/PI Apoptosis Detection kit (Invitrogen) according to the manufacturer's instructions. Finally, the stained cells were subjected to flow cytometry for analysis in 30 min, and 20,000 cells for each sample were examined.

Animal Tumor Models and Treatment. To establish the MV4-11 xenograft model, MV4-11 cells (10^7 cells in 100 μL serum-free IMDM) were injected subcutaneously into the right flanks of 5-6 week old female NOD/SCID mice. As for MM1S xenograft model, MM1S cells (10^7 cells in 100 μL serum-free RPMI 1640) were injected subcutaneously into the right flanks of 5-6 week old female NOD/SCID mice. When the size of the formed xenografts reached 100-200 mm^3, the mice were randomly divided (6 mice per group). In MV4-11 model, the mice in the experimental group received intravenous injection (10 mg/kg, dissolved in physiological saline containing 2.5% DMSO and 10% cyclodextrin with the pH adjusted to 9) of **12l** every 2 days. In MM1S model, those in the SAHA group (positive control) received po treatment (50 mg/kg) was dissolved in physiological saline containing 2.5% DMSO and 10% cyclodextrin with the pH adjusted to 9) every day. And the mice in the SAHA+RAPA group (positive control) received po treatment (50+25 mg/kg) was

equably suspended in physiological saline containing 2.5% DMSO and 10% cyclodextrin with the pH adjusted to 9) every day. Tumor burden was measured every 2 days by a caliper. Tumor volume (TV) was calculated using the following formula: TV =length × width^2 × 0.5. At the end of the experiment, mice were sacrificed and tumors were collected and weighed. The animal studies were conducted in conformity with institutional guide for the care and use of laboratory animals, and all mouse protocols were approved by the Animal Care and Use Committee of Sichuan University (Chengdu, Sichuan, China).

Associated content

Supporting information

Table S1 listing binding affinities of **12l** with various protein kinases; Table S2 listing pharmacokinetic parameters of **12l**; Figure S1 listing western blot in HDAC and mTOR of **12l** and LBH-589. The Supporting Information is available free of charge via the Internet at ACS Publications website.

Molecular formula strings (CSV)

PDB ID CODES

PDB code 5ICN and 4LXZ was used for modeling docking in HDAC1 and HDAC2 of **12l**, respectively; PDB code 4JT6 was used for modeling docking in mTOR. Authors will release the Atomic Coordinates and experimental data upon article publication.

Author contributions

The manuscript was written through contributions of all authors. All authors have

given approval to the final version of the manuscript. Y.C., X.Y., and W.H.Z. contributed equally.

Notes

The authors declare no competing financial interest.

Corresponding Author Information:

*Lijuan Chen. Tel: +86-28-85164063; E-mail address: chenlijuan125@163.com.

*Jun He. E-mail address: Jun_He@scu.edu.cn

ORCID ID

Lijuan Chen: 0000-0002-8076-163X

Jun He: Jun_He@scu.edu.cn

Acknowledgement.

The authors greatly appreciate the financial support from National Key Programs of China during the 13th Five-Year Plan Period (2018ZX09721002-001-004), National Natural Science Foundation of China (81702991), and 1.3.5 project for disiplines of excellence, West China Hospital, Sichuan University.

Abbreviations Used: HDAC, histone deacetylase; PI3Ks, phosphatidylinositol 3-kinases; mTOR, the mammalian target of rapamycin; ZBG, zinc-binding group; SAHA, suberoylanilide hydroxamic acid; RAPA, rapamycin; SAR, structure−activity relationship; MTT, 3-(4,5-dimethylthiazol-2-yl)-2,5-diphenyltetrazolium bromide.

References

1. Verheijen, J. C.; Richard, D. J.; Curran, K.; Kaplan, J.; Lefever, M.; Nowak, P.; Malwitz, D. J.; Brooijmans, N.; Toral-Barza, L.; Zhang, W. G.; Lucas, J.; Hollander, I.; Ayral-Kaloustian, S.; Mansour, T. S.; Yu, K.; Zask, A. Discovery of 4-morpholino-6-aryl-1*H*-pyrazolo[3,4-*d*]pyrimidines as highly potent and selective ATP-competitive inhibitors of the mammalian target of rapamycin (mTOR): optimization of the 6-aryl substituent. *J. Med. Chem.* **2009**, *52*, 8010-8024.

2. Takeuchi, C. S.; Kim, B. G.; Blazey, C. M.; Ma, S.; Johnson, H. W.; Anand, N. K.; Arcalas, A.; Baik, T. G.; Buhr, C. A.; Cannoy, J.; Epshteyn, S.; Joshi, A.; Lara, K.; Lee, M. S.; Wang, L.; Leahy, J. W.; Nuss, J. M.; Aay, N.; Aoyama, R.; Foster, P.; Lee, J.; Lehoux, I.; Munagala, N.; Plonowski, A.; Rajan, S.; Woolfrey, J.; Yamaguchi, K.; Lamb, P.; Miller, N. Discovery of a novel class of highly potent, selective, ATP-competitive, and orally bioavailable inhibitors of the mammalian target of rapamycin (mTOR). *J. Med. Chem.* **2013**, *56*, 2218-2234.

3. Martelli, A. M.; Buontempo, F.; McCubrey, J. A. Drug discovery targeting the mTOR pathway. *Clin. Sci. (Lond)* **2018**, *132*, 543-568.

4. Feldman, M. E.; Apsel, B.; Uotila, A.; Loewith, R.; Knight, Z. A.; Ruggero, D.; Shokat, K. M. Active-site inhibitors of mTOR target rapamycin-resistant outputs of mTORC1 and mTORC2. *PLoS Biol.* **2009**, *7*: e38.

5. Mukherjee, A.; Koli, S.; Reddy, K. V. Rapamycin (Sirolimus) alters mechanistic target of rapamycin pathway regulation and microRNA expression in mouse meiotic spermatocytes. *Andrology* **2015**, *3*, 979-990.

6. Dunlop, E. A.; Tee, A. R. Mammalian target of rapamycin complex 1: signalling

inputs, substrates and feedback mechanisms. *Cell. Signal.* **2009**, *21*, 827-835.

7. Chresta, C. M.; Davies, B. R.; Hickson, I.; Harding, T.; Cosulich, S.; Critchlow, S. E.; Vincent, J. P.; Ellston, R.; Jones, D.; Sini, P.; James, D.; Howard, Z.; Dudley, P.; Hughes, G.; Smith, L.; Maguire, S.; Hummersone, M.; Malagu, K.; Menear, K.; Jenkins, R.; Jacobsen, M.; Smith, G. C.; Guichard, S.; Pass, M. AZD8055 is a potent, selective, and orally bioavailable ATP-competitive mammalian target of rapamycin kinase inhibitor with in vitro and in vivo antitumor activity. *Cancer Res.* **2010**, *70*, 288-298.

8. Willems, L.; Chapuis, N.; Puissant, A.; Maciel, T. T.; Green, A. S.; Jacque, N.; Vignon, C.; Park, S.; Guichard, S.; Herault, O.; Fricot, A.; Hermine, O.; Moura, I. C.; Auberger, P.; Ifrah, N.; Dreyfus, F.; Bonnet, D.; Lacombe, C.; Mayeux, P.; Bouscary, D.; Tamburini, J. The dual mTORC1 and mTORC2 inhibitor AZD8055 has anti-tumor activity in acute myeloid leukemia. *Leukemia* **2012**, *26*, 1195-1202.

9. Mortensen, D. S.; Perrin-Ninkovic, S. M.; Shevlin, G.; Zhao, J.; Packard, G.; Bahmanyar, S.; Correa, M.; Elsner, J.; Harris, R.; Lee, B. G.; Papa, P.; Parnes, J. S.; Riggs, J. R.; Sapienza, J.; Tehrani, L.; Whitefield, B.; Apuy, J.; Bisonette, R. R.; Gamez, J. C.; Hickman, M.; Khambatta, G.; Leisten, J.; Peng, S. X.; Richardson, S. J.; Cathers, B. E.; Canan, S. S.; Moghaddam, M. F.; Raymon, H. K.; Worland, P.; Narla, R. K.; Fultz, K. E.; Sankar, S. Discovery of mammalian target of rapamycin (mTOR) kinase inhibitor CC-223. *J. Med. Chem.* **2015**, *58*, 5323-5333.

10. Xie, J.; Wang, X.; Proud, C. G. mTOR inhibitors in cancer therapy. *F1000Res.* **2016**, *5* : 2078.

11. Rodrik-Outmezguine, V. S.; Okaniwa, M.; Yao, Z.; Novotny, C. J.; McWhirter, C.; Banaji, A.; Won, H.; Wong, W.; Berger, M.; de Stanchina, E.; Barratt, D. G.; Cosulich, S.; Klinowska, T.; Rosen, N.; Shokat, K. M. Overcoming mTOR resistance mutations with a new-generation mTOR inhibitor. *Nature* **2016**, *534*, 272-276.

12. Atadja, P. Development of the pan-DAC inhibitor panobinostat (LBH589): successes and challenges. *Cancer Lett.* **2009**, *280*, 233-241.

13. Wang, H.; Yu, N.; Chen, D.; Lee, K. C.; Lye, P. L.; Chang, J. W.; Deng, W.; Ng, M. C.; Lu, T.; Khoo, M. L.; Poulsen, A.; Sangthongpitag, K.; Wu, X.; Hu, C.; Goh, K. C.; Wang, X.; Fang, L.; Goh, K. L.; Khng, H. H.; Goh, S. K.; Yeo, P.; Liu, X.; Bonday, Z.; Wood, J. M.; Dymock, B. W.; Kantharaj, E.; Sun, E. T. Discovery of (2*E*)-3-{2-butyl-1-[2-(diethylamino)ethyl]-1*H*-benzimidazol-5-yl}-*N*-hydroxyacrylam-ide (SB939), an orally active histone deacetylase inhibitor with a superior preclinical profile. *J. Med. Chem.* **2011**, *54*, 4694-4720.

14. Minucci, S.; Pelicci, P. G. Histone deacetylase inhibitors and the promise of epigenetic (and more) treatments for cancer. *Nat. Rev. Cancer* **2006**, *6*, 38-51.

15. Luan, Y.; Li, J.; Bernatchez, J. A.; Li, R. Kinase and histone deacetylase hybrid inhibitors for cancer therapy. *J. Med. Chem.* **2018**, DOI: 10.1021/acs.jmedchem.8b00189.

16. Yoshida, M.; Kudo, N.; Kosono, S.; Ito, A. Chemical and structural biology of protein lysine deacetylases. *Proc. Jpn. Acad. Ser. B* **2017**, *93*, 297-321.

17. Ganesan, A. Multitarget drugs: an epigenetic epiphany. *ChemMedChem* **2016**, *11*, 1227-1241.

18. Verheul, H. M.; Salumbides, B.; Van Erp, K.; Hammers, H.; Qian, D. Z.; Sanni, T.; Atadja, P.; Pili, R. Combination strategy targeting the hypoxia inducible factor-1α with mammalian target of rapamycin and histone deacetylase inhibitors. *Clin. Cancer Res.* **2008**, *14*, 3589-3597.

19. Oki, Y.; Buglio, D.; Fanale, M.; Fayad, L.; Copeland, A.; Romaguera, J.; Kwak, L. W.; Pro, B.; de Castro Faria, S.; Neelapu, S.; Fowler, N.; Hagemeister, F.; Zhang, J.; Zhou, S.; Feng, L.; Younes, A. Phase I study of panobinostat plus everolimus in patients with relapsed or refractory lymphoma. *Clin. Cancer Res.* **2013**, *19*, 6882-6890.

20. Brandon R. Beagle; Duc. M. Nguyen; Sharmila Mallya; Sarah S. Tang; Mengrou Lu; Zhihong Zeng; Marina Konopleva; Thanh-Trang Vo; David A. Fruman. mTOR kinase inhibitors synergize with histone deacetylase inhibitors to kill B-cell acute lymphoblastic leukemia cells. *Oncotarget* **2014**, *6*, 2088-2100.

21. Li Hua Dong; Shu Cheng; Zhong Zheng; Li Wang; Yang Shen; Zhi Xiang Shen; Sai Juan Chen; Wei Li Zhao. Histone deacetylase inhibitor potentiated the ability of mTOR inhibitor to induce autophagic cell death in Burkitt leukemia/lymphoma. *J. Hematol. Oncol.* **2013**, *6* : 53.

22. Wedel, S.; Hudak, L.; Seibel, J. M.; Makarevic, J.; Juengel, E.; Tsaur, I.; Wiesner, C.; Haferkamp, A.; Blaheta, R. A. Impact of combined HDAC and mTOR inhibition on adhesion, migration and invasion of prostate cancer cells. *Clin. Exp. Metastasis.* **2011**, *28*, 479-491.

23. Malone, C. F.; Emerson, C.; Ingraham, R.; Barbosa, W.; Guerra, S.; Yoon, H.;

Liu, L. L.; Michor, F.; Haigis, M.; Macleod, K. F.; Maertens, O.; Cichowski, K. mTOR and HDAC inhibitors converge on the TXNIP/Thioredoxin pathway to cause catastrophic oxidative stress and regression of RAS-driven tumors. *Cancer Discov.* **2017**, *7*, 1450-1463.

24. Amila Suraweera; Kenneth J. O'Byrne; Derek J. Richard. Combination therapy with histone deacetylase inhibitors (HDACi) for the treatment of cancer: achieving the full therapeutic potential of HDACi. *Front. Oncol.* **2018**, *8* : 92.

25. Gupta, M.; Ansell, S. M.; Novak, A. J.; Kumar, S.; Kaufmann, S. H.; Witzig, T. E. Inhibition of histone deacetylase overcomes rapamycin-mediated resistance in diffuse large B-cell lymphoma by inhibiting Akt signaling through mTORC2. *Blood* **2009**, *114*, 2926-2935.

26. Emily K. Slotkin; Parag P. Patwardhan; Shyamprasad D.Vasudeva; Elisa de Stanchina; William D. Tap; Gary K. Schwartz. MLN0128, an ATP-competitive mTOR kinase inhibitor with potent in vitro and in vivo antitumor activity, as potential therapy for bone and soft tissue sarcoma. *Small Mol. Ther.* **2015**, *14*, 395-406.

27. Haggarty, S. J.; Koeller, K. M.; Wong, J. C.; Grozinger, C. M.; Schreiber, S. L. Domain-selective small-molecule inhibitor of histone deacetylase 6 (HDAC6)-mediated tubulin deacetylation. *Proc. Natl. Acad. Sci. U.S.A.* **2003**, *100*, 4389-4394.

28. Chen, Y.; Wang, X.; Xiang, W.; He, L.; Tang, M.; Wang, F.; Wang, T.; Yang, Z.; Yi, Y.; Wang, H.; Niu, T.; Zheng, L.; Lei, L.; Li, X.; Song, H.; Chen, L. Development of purine-based hydroxamic acid derivatives: potent histone deacetylase inhibitors

with marked in vitro and in vivo antitumor activities. *J. Med. Chem.* **2016**, *59*, 5488-5504.

29. Younes, A.; Samad, N. Utility of mTOR inhibition in hematologic malignancies. *Oncologist* **2011**, *16*, 730-741.

30. Yang, Z.; Wang, T.; Wang, F.; Niu, T.; Liu, Z.; Chen, X.; Long, C.; Tang, M.; Cao, D.; Wang, X.; Xiang, W.; Yi, Y.; Ma, L.; You, J.; Chen, L. Discovery of selective histone deacetylase 6 inhibitors using the quinazoline as the cap for the treatment of cancer. *J. Med. Chem.* **2016**, *59*, 1455-1470.

31. Dos D. Sarbassov; Siraj M. Ali; Shomit Sengupta; Joon-Ho Sheen; Peggy. P. Hsu; Alex F. Bagley; Andrew L. Markhard; David M. Sabatini. Prolonged rapamycin treatment inhibits mTORC2 assembly and Akt/PKB. *Mol. Cell* **2006**, *22*, 159-168.

32. Chen, X.-G.; Liu, F.; Song, X.-F.; Wang, Z.-H.; Dong, Z.-Q.; Hu, Z.-Q.; Lan, R.-Z.; Guan, W.; Zhou, T.-G.; Xu, X.-M.; Lei, H.; Ye, Z.-Q.; Peng, E. J.; Du, L.-H.; Zhuang, Q.-Y. Rapamycin regulates Akt and ERK phosphorylation through mTORC1 and mTORC2 signaling pathways. *Mol. Carcinogen.* **2010**, *49*, 603-610.

33. Fingar, D. C.; Richardson, C. J.; Tee, A. R.; Cheatham, L.; Tsou, C.; Blenis, J. mTOR controls cell cycle progression through its cell growth effectors S6K1 and 4E-BP1/eukaryotic translation initiation factor 4E. *Mol. Cell. Biol.* **2003**, *24*, 200-216.

34. Watson, P. J.; Millard, C. J.; Riley, A. M.; Robertson, N. S.; Wright, L. C.; Godage, H. Y.; Cowley, S. M.; Jamieson, A. G.; Potter, B. V. L.; Schwabe, J. W. R. Insights into the activation mechanism of class I HDAC complexes by inositol phosphates. *Nat. Commun.* **2016**, *7* : 11262.

35. Lauffer, B. E.; Mintzer, R.; Fong, R.; Mukund, S.; Tam, C.; Zilberleyb, I.; Flicke, B.; Ritscher, A.; Fedorowicz, G.; Vallero, R.; Ortwine, D. F.; Gunzner, J.; Modrusan, Z.; Neumann, L.; Koth, C. M.; Lupardus, P. J.; Kaminker, J. S.; Heise, C. E.; Steiner, P. Histone deacetylase (HDAC) inhibitor kinetic rate constants correlate with cellular histone acetylation but not transcription and cell viability. *J. Biol. Chem.* **2013**, *288*, 26926-26943.

36. Yang, H.; Rudge, D. G.; Koos, J. D.; Vaidialingam, B.; Yang, H. J.; Pavletich, N. P. mTOR kinase structure, mechanism and regulation. *Nature* **2013**, *497*, 217-223.

Table of Contents Graphic

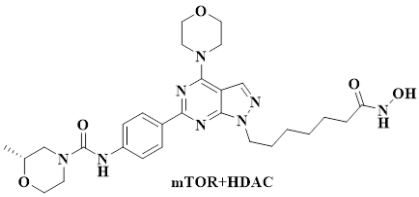

mTOR+HDAC

HDAC1	0.19 nM
HDAC6	1.8 nM
mTOR	1.2 nM
PI3Kα	> 500 nM